

**Mineralogical and geochemical characterisation of warm water,  
shallow marine glaucony from the Tertiary of the London Basin**

Jennifer Huggett<sup>1,2,\*</sup>, Jacob Adetunji<sup>3</sup>, Fred Longstaffe<sup>4</sup> and David  
Wray<sup>5</sup>

<sup>1</sup> Oast House, Sandy Cross, Heathfield, E Sussex, TN21 8QP;

<sup>2</sup> The Natural History Museum, London, SW7 5BD, UK

<sup>3</sup> Department of Natural Science, University of Derby, DE22 1GB, UK

<sup>4</sup> Department of Earth Sciences, The University of Western Ontario,  
London, N6A 5B7, Canada;

<sup>5</sup> Department of Pharmaceutical, Chemical and Environmental  
Sciences, University of Greenwich, ME4 4TB, UK;

\*Corresponding author e-mail address: [info@petroclays.com](mailto:info@petroclays.com)

**Abstract**

Glaucony is present in the Palaeocene sediments of the London  
Basin, from the Thanet Sand Formation to the gravel beds at the

base of the Lower Mottled Beds of the Reading Formation. The Upnor Formation glaucony is a rare example of formation in warm, shallow brackish water and this, combined with the ready availability of fresh material from boreholes, make this study important in developing our understanding of this mineral. Glaucony comprises up to 50% of the Upnor Formation, a grey to green sandstone, of variable thickness and composition, that was deposited in a warm, shallow marine to estuarine environment, ~55.6-56.2 Ma. Using morphological criteria, X-ray diffraction data and  $K^+$  abundance, the Upnor glaucony may be defined as evolved. The underlying shallow marine Thanet Sand contains <5% of nascent to slightly evolved glaucony. The REE data for the Upnor Formation suggest more than one source for the sediment from which the Upnor glaucony formed, while the Thanet REE data are consistent with a high detrital clay component.

In the Upnor Formation, the high proportion of glaucony that occurs as granule fragments rather than whole granules, and the high-energy estuarine to shallow marine environment of deposition, are indicative of reworking. The Upnor glaucony is inferred to be intraformationally reworked, rather than derived from the Thanet Sand Formation. The glaucony may have formed in sediments deposited away from the main estuarine channel, and been

subsequently reworked into higher energy sediments. Warm seas with freshwater mixing are more typically characteristic of verdine formation than of glaucony. The shallow, brackish environment of deposition suggests that there is not a clear distinction between the environmental requirements of verdine (or odinite) and glaucony (or glauconite), as is often proposed. The highly fractured, delicate nature of some granules indicates that they have experienced some maturation *in situ*, after reworking.

The oxygen and hydrogen isotopic compositions of Upnor Formation shark teeth and glaucony point to formation in low salinity water at  $\sim 23 \pm 3^\circ\text{C}$ , also consistent with formation in the Upnor Formation, rather than in a fully marine sediment and subsequent reworking. A higher than normal temperature of formation may have increased the rate of evolution of glaucony.

Our multidisciplinary study considers many of the factors relating to depositional environment that must be considered when glaucony-rich facies are encountered in comparable palaeoenvironmental settings elsewhere in the geological record.

Key words: Glaucony formation; glauconite weathering; Upnor Formation; oxygen isotope analysis; REE; Mössbauer spectroscopy; Fe-ion distribution

## INTRODUCTION

The petrographic facies in which glauconitic minerals are abundant has been termed the glaucony facies (Odin & Stephan, 1981; Odin & Matter, 1981). The term glaucony is typically used to denote the entire range of olive-green to dark green clay granules, such as are encountered in the Upnor and Reading Formations, while the term glauconite is reserved for an iron-rich dioctahedral mica (Bailey, 1980). Glauconitic clay ranges from the “immature” smectite-rich end member to the “highly evolved” mica-rich end member. Four stages of glauconitisation were first characterised by Odin & Matter (1981), based on the petrographic characteristics of the granules. Odin & Fullager (1988) (their Fig. 12) further developed this categorisation by adding  $K_2O$  content to the definitions: nascent  $<4\%$   $K_2O$ , slightly evolved  $4-6\%$   $K_2O$ , evolved  $6-8\%$   $K_2O$  (with fractures resulting from dehydration of the clay), and highly evolved  $>8\%$ .

Glaucy typically develops by replacement of pseudofaecal pellets in surficial marine sediments, and is most notably abundant in transgressive sands (e.g. McRae, 1972; Odin & Fullagar, 1988; Huggett & Gale, 1997). The degree of glauconitisation is perceived to be an indication of the duration, in relative terms, of a period of very slow, or zero sedimentation. In order to correctly interpret the significance of glaucy it is essential to establish whether a deposit is *in situ* (Huggett & Gale, 1997; Huggett & Laenen, 1996; Kelly & Webb, 1999). Criteria for determining whether glaucy is reworked include the presence of fragments of glaucy, and winnowing of glaucy into laminae. The presence of glaucy in burrow fills is regarded as evidence of *in situ* glauconitisation. Reworked pellets may continue to mature after reworking, e.g. reworked fragments may develop fractures.

Most of the available material is from the Upnor Formation, and this is reflected in the data presented here. The objectives of this investigation are to characterise the glauconitic clays of the Thanet Sand formation and Lambeth Group, in the sub-surface and outcrop of southern England (Fig. 1), to determine: (i) the extent to which these granules formed *in situ*, (ii) their environment of formation, and (iii) the effect of pedogenic weathering on glaucy. The majority of glaucy occurrences are in outer shelf sediments, in water depths

considerably greater than those of the Upnor Formation. Hence either the Upnor glaucony has been reworked into shallow water, or it has been deposited in unusually shallow water, in environments more generally associated with verdine (Odin & Sen Gupta, 1988; Odin et al., 1988).

## **GEOLOGICAL BACKGROUND**

The principal object of this study, the Upnor Formation (basal formation of the Lambeth Group, ~55.6-56.2 Ma, nannoplankton zones NP8-NP9) is a glauconitic sandstone that rests unconformably on the sparsely glauconitic Thanet Sand Formation in the London basin (Fig. 2). The Thanet Sand Formation is a fully marine, shelf sand (Ellison et al., 2004). Between deposition of the Thanet Sand and the Upnor formations there was a fall in sea level and a break in sedimentation. The Lambeth Group comprises three depositional sequences (Fig. 2). Following a significant rise in sea level at ~56.2 Ma (Ali & Jolley, 1996), Upnor Formation sediments were deposited in a shallow marine (Sequence 1) to estuarine (Sequence 2) environment, over an area extending from East Kent to Wiltshire

approximately 150 miles to the west. Heavy mineral studies suggest a southerly, Armorican (Lower Palaeozoic) source for the sediment (e.g. Blondeau & Pomerol, 1968, Weir & Catt, 1969, Morton, 1982). In the eastern part of the London Basin there is evidence of erosion of the upper Thanet Sand Formation, where overlain by the Upnor Formation (Morton, 1982; King, 2016).

Ellison et al. (1996) and Knox (1996) recognise two units in the Upnor Formation, with a break of ~0.1 Ma between them, during which time uplift, tilting and local erosion occurred. In North Kent both units are present, while in parts of central London the upper unit appears to have been eroded (Ali & Jolley, 1996; Newman, 2013), though the quality of the borehole material is not always adequate to accurately identify the stratigraphy. In the London Basin, the lower unit contains an abundant and diverse microplankton flora, typical of a relatively normal shallow marine setting. The upper unit contains a sparse microplankton flora with assemblages suggestive of a marine environment with high stress, such as a lower- than-normal salinity (Powell et al., 1996; Skipper, 1999), or rising global temperatures in the interval leading up to the Paleocene-Eocene Maximum (PETM) (Sluijs et al., 2006; Zacke et al., 2009; Zachos et al., 2010; Kemp et al., 2016). Lower salinity in this environment has been attributed to uplift to the north, resulting in excessive freshwater runoff and

surface freshening of the North Sea (Powell et al., 1996; Zacke et al., 2009). The pollen and spore assemblages are impoverished and dominated by *Pityosporites* spp. (Powell et al., 1996), a microspore that might have been concentrated by winnowing in a relatively high-energy, nearshore environment.

The Upnor Formation is typically 5-8 m thick, locally as much as 15 m, decreasing to <2 m westwards (King, 2012; 2016). A basal bed of rounded flint pebbles is usually present, passing up into variably bioturbated (*Ophiomorpha* and *Macaronichnus*) fine to medium grained sandstone with a variable proportion of silty clay matrix and glauconitic granules, plus thin beds and stringers of flint pebbles, passing up into a further pebble bed at the top of the formation (Ellison et al., 2004). In clay-rich units, up to 0.3 m thick sand laminae highlight flaser lamination, and lenticular cross-lamination. In the west and some central parts of the London Basin the Upnor Formation is distinctly green, reflecting a relatively high glaucony content (Ellison et al., 2004). In the Jubilee Line borehole T404, four glaucony maxima have been identified in ~6 m of Upnor Formation (Ellison et al., 1996), though these do not clearly correspond to changes in lithology or sedimentary structure. At Charlton pit, in East London, two glaucony maxima are visible. Elsewhere trends in glaucony abundance are difficult to identify, mainly due to a lack of

exposure and poor stratigraphic control for borehole material. In north Kent the Upnor Formation is generally heterogeneous, with clay streaks and *Ophiomorpha* burrows, and is partly cross-bedded with gravel at the base (King, 2012). At Herne Bay, the Upnor Formation is a bioturbated, sparsely glauconitic, very fine-grained, clayey sandstone with occasional gravel (none seen during sampling). The basal bed at Herne Bay, the Beltinge Fish Bed, has a fully marine flora and fauna (Ward, 1978). In southeast Kent, around Canterbury, the Upnor Formation is more glauconitic than in north Kent (King, 2012; 2016).

The upper part, and locally in the north, west and central parts of the area of deposition, all of the Upnor Formation is oxidised to a range of brown, red, orange and purple-brown colours as a result of emergence and pedogenesis during deposition of the overlying Reading Formation (Lambeth Group, 55-55.6 ma). Glaucony persists in an increasingly weathered form into the non-marine Lower Mottled Beds (LMB) of the Reading Formation. Unweathered glaucony is particularly abundant in the gravel bed at the base of the LMB. Sparse powdery carbonate concretions in the Upnor Formation may have formed during this period of pedogenesis, and clay matrix may have been derived by translocation from the overlying deposits (Ellison et al., 2004).

In broad terms, the Upnor Formation may be regarded as representing the transgressive phase of the Lambeth Group, with the overlying Reading and Woolwich formations representing maximum flooding, followed by exposure and weathering during the high stand phase (Knox, 1996). In the lower Upnor unit, there was connection with the oceanic waters of the eastern Atlantic (Hine, 1994). This period of oceanic connection was short-lived as result of uplift to the southwest, with the upper Upnor unit representing a change to restricted marine to estuarine conditions throughout the Anglo-Paris basin. This uplift is represented by a pebble bed in the central London area, and to the east by laminated clayey sands, deposited as estuarine or shallow marine sediment (Skipper, 1999; King, 2012). The eastern most sample locality, Herne Bay in north Kent, is an example of an area where the uplift is represented by shallow marine sediment; the London bore holes (Fig. 1), by comparison, are within the area represented by a pebble bed. Subsequently, in western parts of the area, restricted marine or lagoonal environments, represented by coarsely glauconitic sands, became established, whereas littoral to sublittoral environments, represented by relatively thick, less glauconitic sands, and local conglomerates, developed in the east (Knox, 1996). In many parts of the London Basin, subsequent erosion has removed the upper Upnor unit (Newman,

2013).

## METHODS

Eighty samples from the Upnor Formation, including the pedogenically weathered mottled Upnor were obtained from fourteen Thames Water boreholes, from outcrop at Herne Bay in east Kent and from the Jubilee Underground Line extension borehole T404 (Fig 1). Six samples of glauconitic Thanet Sand Formation were also analysed to assess whether the Upnor Formation glaucony is sufficiently similar to have been derived from the older Thanet Sand Formation glaucony. Borehole samples were selected to give maximum possible east to west coverage. Closely spaced, stratigraphically well-constrained samples were obtained from the Abbey Mills and T404 boreholes, to assess the vertical variability of the formation. The extreme lateral variability of the Upnor Formation from borehole to borehole across the London Basin does not facilitate accurate stratigraphic location of samples (Newman, 2013). For this reason samples from boreholes other than Abbey Mills and T404 are identified as coming from the top, upper, middle, lower or base of the Upnor Formation, according to the sample depth relative

to the known thickness of the Upnor Formation at that location. Present burial depths of the sampled intervals vary from approximately 25-40m. As these are the maximum burial depths there is no reason to suspect post-burial diagenetic alteration of the glaucony. At Herne Bay samples were collected from the foreshore exposure: the Beltinge Fish Bed ~ 0.05m above the base (sample C), ~0.02m above the base (sample D), ~1.5m above the base (sample B) and ~2.0m from the top (sample A). Because the exposure is partially covered with beach sediment, these exposure depths are approximate.

Petrographic examination, X-ray diffraction analysis (XRD), Inductively coupled plasma - optical emission spectroscopy and – mass spectrometry (ICP-OES & -MS), Mossbauer spectroscopy and oxygen- and hydrogen-isotope analyses were performed on magnetically separated glaucony. In addition, XRD was performed on the clay matrix of selected samples. Glaucony grains were separated from sand and clay by first sieving out the >63  $\mu\text{m}$  fraction. The >63  $\mu\text{m}$  fraction was briefly treated ultrasonically to remove any remaining detrital clay from granule surfaces. The glaucony was then separated from the non-magnetic fraction (mainly quartz) using a Frantz Magnetic Separator. Purity of the glaucony was checked using a binocular microscope, and remaining visible quartz grains removed.

Weathered glaucony could not be separated from the enclosing matrix because of the highly friable nature of the altered granules.

#### *Petrography and Electron Microscopy*

Glaucony abundances were determined by optical microscopy, point-counting 300 points per thin section. Polished thin sections were examined optically and in back-scattered electron-imaging mode, using a Zeiss EVO SEM equipped with an Oxford Instruments INCA energy dispersive spectral (EDS) X-ray spectrometer. EDS analyses were obtained for both weathered and unweathered granules.

Operating conditions were a 2  $\mu$ A beam current at 15 kV accelerating voltage, and a spot diameter of approximately 2  $\mu$ m. Detection limits vary according to the analysed elements and the matrix in which they are contained. For these samples detection limits are 0.2% for Mg, Ca, and K, 0.4-0.6% for Al, Si, P, Mn, Ti, and Fe. Calibration using a cobalt standard was performed prior to analysis, and the beam current was monitored during analysis. The mean unweathered glaucony composition was determined by averaging the EDS analyses for each sample.

#### *X-Ray Diffraction*

Powder samples of disaggregated and lightly ground granules were scanned at a rate of 15 seconds per  $0.05^\circ 2\theta$  step width using a  $0.5^\circ$  slit, from  $5$  to  $70^\circ 2\theta$ . For  $<2\ \mu\text{m}$  clay fraction analysis of the glaucony, a portion of glaucony granules was gently crushed by hand, fully dispersed in water by placing in an ultrasonic bath for 30 minutes, and the  $<2\ \mu\text{m}$  fraction separated by centrifugation.. Whilst it is recognised that the glaucony contains particles  $>2\ \mu\text{m}$ , the  $<2\ \mu\text{m}$  fraction forms the greater part of the dispersed granules, and yields XRD results that are consistent with the chemical data obtained for the whole granules. The  $<2\ \mu\text{m}$  fraction was prepared as an oriented clay mount and analysed using a Phillips 1820 automated X-ray diffractometer equipped with Ni-filtered  $\text{CuK}\alpha$  radiation. Clay tiles were scanned at a rate of 5 seconds per  $0.02^\circ$  step width, using 0.3 mm slits from  $2$  to  $40^\circ 2\theta$ . The tiles were scanned again after ethylene glycol solvation for two hours, heating at  $400^\circ\text{C}$  for 4 hours, after heating at  $550^\circ\text{C}$ , also for 4 hours. The  $<2\ \mu\text{m}$  fraction of the clay matrix separated during glaucony extraction was analysed following the same procedure. For the weathered samples, XRD analysis of the clay fraction was carried out on the combined matrix and weathered granules. Peak deconvolution and area measurement were carried out using MacDiff 4.26 (<http://www.geol-pal.uni->

[frankfurt.de/Staff/Homepages/Petschick/MacDiff/MacDiffInfoE.html](http://frankfurt.de/Staff/Homepages/Petschick/MacDiff/MacDiffInfoE.html)).  
Semi-quantitative measurement of the % 0.1 nm micaceous layers in the glauconite-smectite was made for the ethylene glycol solvated scans using Table 7.3 in Moore & Reynolds (1989).

### *ICP-OES & -MS*

Major, trace, and rare-earth element (REE) data were derived from samples after dissolution via lithium metaborate fusion (see Wray & Wood, 1998, for method) and quantification by a combination of ICP-OES (Thermo iCAP 6500) and ICP-MS (Thermo X Series 2) at the University of Greenwich ISO17025 accredited laboratory (testing lab 2180). Calibration was performed via matrix matched, traceable synthetic standards. QA/QC protocols included the analysis and charting of in-house QC samples and the analysis of a series of geological reference materials at regular intervals through the analytical sequence. Prior to plotting, REE data were normalized to the values derived from analysis of USGS reference material Cody Shale (SCo-1), which is considered to have a chemical composition representative of average shale (Jarvis & Jarvis, 1985). Cody shale was also included in the analytical schedule to minimize subtle analytical artefacts that may occur if numeric values for average

shale (such as PAAS) are used.

### *Mössbauer Spectroscopy*

The room temperature Mössbauer spectroscopy experiment was carried out at the University of Derby using a MS-2 spectrometer manufactured by the Centre for Advanced Technologies and Materials, Olomouc, Czech Republic. Each absorber was prepared from 68.0 mg of glaucony, mixed with boron nitride as a binder. The mixture was spread uniformly over an area of  $\sim 1.8\text{cm}^2$ , and pressed into a pellet. The spectrum was recorded with a 25 mCi  $^{57}\text{Co}$  (in Rhodium matrix) source mounted on a constant-acceleration transducer operated in a triangular mode in a velocity range,  $\pm 6$  mm/s. The Doppler energies from the 14.4keV  $\gamma$ -rays were detected with a  $\text{YAlO}_3\text{:Ce}$  scintillation counter. The data was recorded in 1024 channels, which covers twice the Doppler velocity range. Spectra were calibrated against a high purity (99.99%) natural  $\alpha$ -Fe foil and all peak positions reported with respect to the centroid shift (CS) of the natural  $\alpha$ -Fe. Lorentzian lines of the folded data were fitted, using the least-square RECOIL 1.04 Mössbauer Spectral Analysis Software developed by Lagarec & Rancourt (1998). Reduced  $\chi^2$  was used as a parameter to evaluate the statistical best-fit of the spectra

and uncertainties were calculated using a covariant matrix. The oxidation states of Fe-ions were then characterized by the centroid shift and site occupancy determined by the area ratios of the spectral doublets.

### *Oxygen-, hydrogen- and carbon-isotopes*

All stable isotopic analyses were carried out in the Laboratory for Stable Isotope Science (LSIS) at the University of Western Ontario, and are reported in the standard  $\delta$ -notation relative to VSMOW for oxygen and hydrogen, and VPDB for carbon using two-point calibrations following Coplen (1996) and Coplen et al. (2006). Results reported for accuracy (see below) exclude standards used to anchor the calibration curves.

To obtain glaucony oxygen isotopic analyses, ~8 mg of sample powder were placed into spring-loaded sample holders, which were then heated at 150°C for 12 hours under dynamic pumping. The samples were then top-loaded into nickel reaction vessels, where they were heated at 150°C for a further 3 hours under dynamic pumping. Chlorine trifluoride was then added to the nickel reaction vessels, and the vessels sealed and reacted for 16 hours at 580°C to release the silicate-bound oxygen; the oxygen was recovered and quantitatively converted to CO<sub>2</sub> for oxygen isotope analysis (Clayton & Mayeda, 1963; Borthwick & Harmon, 1982). The

oxygen isotopic results were measured using a VG Optima dual-inlet stable-isotope-ratio mass-spectrometer (IRMS). The following average  $\delta^{18}\text{O}$  ( $\pm\text{SD}$ ) was obtained for replicate analyses of standards analysed during the course of these measurements (n and accepted value in parentheses): laboratory standard quartz (n = 6),  $+11.6 \pm 0.1 \text{ ‰}$  (+11.5 ‰); kaolinite standard KGa-1 (n = 8),  $+21.4 \pm 0.1 \text{ ‰}$  (+21.5 ‰), and laboratory standard carbon dioxide (n = 8),  $+10.29 \pm 0.08 \text{ ‰}$  (+10.30 ‰). An average reproducibility of  $\pm 0.2 \text{ ‰}$  (n = 6) was obtained for duplicate analyses of glaucony samples.

To obtain glaucony hydrogen isotopic analyses, structural hydrogen was extracted from glaucony using a method modified after Godfrey (1962), Kyser & O'Neil (1984) and Venneman & O'Neil (1993). Briefly, ~70 mg of glaucony was loaded into a quartz tube and outgassed for 12 hours at 200°C to remove adsorbed and interlayer water. The sample was then heated using a fuel-gas-oxygen torch for ~10 minutes during which released H<sub>2</sub>O was trapped at -196°C. Gas initially released as H<sub>2</sub> was oxidized over CuO at 550°C to form H<sub>2</sub>O, which was also collected in the -196°C trap. The total water collected was reacted with powdered chromium at 900°C to produce H<sub>2</sub>, which was collected on charcoal at -196°C. The H<sub>2</sub> was analysed using a Thermo Scientific™ Delta<sup>PLUS</sup>XL dual inlet IRMS. The following average  $\delta^2\text{H}$  ( $\pm\text{SD}$ ) was obtained for replicate analyses of standards during the course of these measurements

(accepted value in parentheses): standard 'Mid' laboratory water (n = 2),  $-107.5 \pm 0.1$  ‰ ( $-108.1$  ‰); standard 'EDT' laboratory water (n = 2),  $-59.1 \pm 2.1$  ‰ ( $-56$  ‰), and kaolinite KGa-1 (n = 5),  $-59.7 \pm 2.0$  ‰ ( $-57$  ‰). An average reproducibility of  $\pm 1.4$  ‰ (n = 3) was obtained for duplicate analyses of glaucony samples.

To obtain phosphate oxygen isotope analyses of shark tooth enameloid, ~30-35 mg of powder from each sample was dissolved in 3 M acetic acid. Silver phosphate ( $\text{Ag}_3\text{PO}_4$ ) was then precipitated through several chemical intermediaries (lead phosphate, lead sulphate) following the ammonia volatilization method (Firsching, 1961; Stuart-Williams & Schwarcz, 1995). About ~0.2 mg of powdered  $\text{Ag}_3\text{PO}_4$  was then loaded into silver capsules and introduced into a Thermo Scientific™ High Temperature Conversion Elemental Analyzer (TC/EA) using a zero blank autosampler. Following reaction at  $1350^\circ\text{C}$  for a few seconds with the TC/EA glassy carbon tube, the resulting carbon monoxide (CO) gas was passed through a heated ( $90^\circ\text{C}$ ), homemade GC column packed with a .5 nm molecular sieve to eliminate impurities such as water vapour. The CO was then swept using helium-2% hydrogen gas in continuous flow mode to a Thermo Scientific Delta<sup>PLUS</sup>XL IRMS for isotopic analysis, where its oxygen isotopic composition was measured. The following average phosphate  $\delta^{18}\text{O}$  ( $\pm\text{SD}$ ) was obtained for replicate analyses of NBS 120c (n = 5) during the course of these measurements (accepted value in

parentheses):  $+21.74 \pm 0.22$  ‰ ( $+21.7$  ‰). Reproducibility of better than 0.1 ‰ ( $n = 2$ ) was obtained for duplicate analyses of separate extractions of enameloid phosphate oxygen.

To obtain stable isotopic analyses for oyster shells,  $\sim 0.05$  mg of powdered Ca-carbonate was reacted with orthophosphoric acid ( $\text{H}_3\text{PO}_4$ ) at  $90^\circ\text{C}$  for 10 minutes using a Micromass Multiprep autosampling device. The resulting  $\text{CO}_2$  was then purified cryogenically and then automatically transferred on-line to a VG Optima dual-inlet IRMS for oxygen and carbon isotopic measurements. The following  $\delta^{18}\text{O}$  was obtained for standards during the course of these measurements (accepted value in parentheses): WS-calcite,  $+26.31$  ‰ ( $+26.23$  ‰); SupraPur,  $+13.42$  ‰ ( $+13.30$ ). For  $\delta^{13}\text{C}$ , results for standards were: WS-calcite,  $+0.88$  ‰ ( $+0.76$  ‰); NBS-18,  $-5.02$  ‰ ( $-5.0$  ‰); SupraPur,  $-35.48$  ‰ ( $-35.55$  ‰). Reproducibility of better than 0.2 ‰ ( $n = 2$ ) was obtained for duplicate oxygen and carbon isotope analyses of separate extractions of oyster shell calcium carbonate.

## RESULTS

### *Petrography*

The Upnor Formation is a clay-rich, silty sandstone, with localized

claystone and siltstone laminae. Glaucony abundance varies widely both within and between the Upnor and Reading formations (deposited data EDS). In the Thanet Formation, glaucony is scarce (<5%), and comprises olive-brown (nascent) to olive-green (slightly evolved to evolved), mostly entire (i.e. not fragmented) granules. Of the sampled Upnor Formation localities, only at Herne Bay is glaucony a minor component (<5%) throughout. In the Upnor Formation glaucony granule abundance varies from trace to ~30% (modal analysis of 25 London borehole samples), while in the gravel bed at the base of the LMB, unweathered glaucony is 0~55% of the sediment (modal analysis of 30 samples), and in the clay-poor Thanet Sand Formation glaucony abundance is <5%. In the top few Upnor Formation samples from borehole T404, Shadwell and Chambers Wharf, finely disseminated silt and clay-grade glaucony give the entire sediment a homogeneously green colour. The distribution of glaucony granules within samples is apparently random, with no concentrations of granules in laminae or burrow fills. Above the gravel bed, glaucony is (now) absent. In both the Upnor and Reading formations, the glaucony occurs as a mixture of round granules, highly fractured granules and fragments of granules, with no primary granule textures apparent other than occasional vermiform structures (Fig. 3a). These features are consistent with the

glaucy being at the evolved stage defined by Odin & Matter (1981). Glaucy granules are typically 0.5-1.5 mm in diameter; granule fragments are up to 0.7 mm. There is a gradation from samples with mostly entire granules and just a few fragments (Fig. 3b), to samples with a matrix of silt-size fragments, or, in just a few samples, a matrix of disaggregated granules (Fig. 3c). In lightly weathered LMB, green granules of unweathered glaucy occur in a goethite-rich matrix (Fig. 3d).

No unequivocally *in situ* (e.g. burrow lining) glaucy was detected, though the existence of highly fractured granules indicates *in situ* evolution of the granules (Fig. 4a). The glaucy is variably reworked. Identification of granule reworking cannot be precise because granules can be undamaged by the process, making it difficult to tell distinguish reworked from un-reworked granules in optical or BSEM images. EDS analyses of inclusions in the glaucy pellets indicate that the majority are Ti oxide, with occasional grains of phosphate that are rich in HREE, most notably in the Herne Bay Beltinge Fish Bed and the Blackfriars boreholes in central London. The Thanet Sand Formation glaucy ranges from nascent to slightly evolved (Fig. 4b).

#### *X-ray diffraction*

The <2  $\mu\text{m}$  fraction of the unweathered Upnor and LMB glaucony granules comprises glauconite, with minor or trace illite, kaolinite and a thermally-resistant 0.7nm component, most likely berthierine (Fig. 5a). Glauconite is distinguished from illite using the position of the 060 diffraction peak (0.1511 nm for glauconite, 0.1503-0.1499 for illite; data from the compilations in Brindley & Brown, 1980), and the weak to absent 002 diffraction peak in glauconite. In all granule separates (whole sample powder analysis and <2  $\mu\text{m}$  oriented mount), the 002 diffraction is weak or absent, from which it is inferred that illite is a negligible component of these granules. The 060 diffraction was measured on 20 of the powder diffraction traces, giving an average value of 0.1511 nm for the Upnor and Reading formation glaucony. A slight shift to lower angles after glycol solvation indicates the presence of a small proportion of smectite layers in the <2  $\mu\text{m}$  fraction of the unweathered green granules (Fig. 5a). The glauconite-smectite mixed-layer clay has a variable composition, indicated by the peak widths, but using the method of Moore & Reynolds (1989) the modal value is calculated to be <10% smectite, >90% 1 nm layers. These deductions from XRD data are consistent with the petrographic interpretation that the Upnor Formation glaucony granules are at the evolved stage of maturation. The <2  $\mu\text{m}$  fraction of the glaucony from the Thanet Formation has a

much higher proportion of smectite layers and lower proportion of 1 nm layers (Fig. 5b), with calculated 1 nm values of 44-51%. These values for smectite indicate that the less evolved granules survived the vigorous sieving during purification of the glaucony fraction for XRD analysis.

There is no systematic trend in glaucony maturity as measured by the glauconite-smectite composition of the Upnor and Reading formation granules, across London, from east (boreholes, Tower Bridge 1, Shadwell) to west (boreholes Vauxhall A and B) (deposited data EDS). Nor is there any east to west trend when the more easterly (more marine) Herne Bay data are included. No vertical trend in the mineralogical composition of the glaucony granules was found for either the Abbey Mills shaft or for borehole T404. For other locations, too few samples were available to detect any vertical mineralogical trends. The high smectite content of the granules at the top of T404 corresponds to the interval where the granules have been extensively reworked, and probably sub-aerially exposed, given that some goethite is present. The smectite content is not therefore an indication of lower maturity.

Throughout the succession, the clay fraction of the matrix in the Upnor Formation is dominated by smectite-rich illite-smectite, with minor illite, plus rare kaolinite and chlorite. The Reading Formation

matrix is similar, but with the addition, goethite, lepidocrocite and gibbsite. Samples that are homogeneously green owing to the presence of silt-size fragments of glaucony have a very slightly higher smectite content than samples with granules. In the lower part of the LMB, immediately above the Upnor Formation, unweathered green granules (i.e. no smectite layers or iron oxyhydroxides detected in their XRD analysis) occur in a brown, goethite-rich matrix. In the most weathered samples of the upper part of the LMB, the presence of glaucony can only be detected as sub-circular outlines in ferruginous clay. It was not possible therefore to physically separate the matrix and the weathered granules. The combined matrix and weathered glaucony granules are dominated by smectite-rich illite-smectite with minor illite, kaolinite and chlorite.

#### *Mössbauer Spectroscopy*

The Mössbauer spectroscopic method is sensitive to local variations in cation distribution in the particular spectra of minerals such as glauconite with widely developed isomorphic substitutions and low crystallinity. The interpretation of their spectra is not straight forward because of vacant *trans*- octahedral sites and wide variation of chemical composition (Drits, 1997). The  $Fe^{2+}/\Sigma Fe$  ratio calculations were based on the intensity ratios of the corresponding spectral lines, on the assumption that, at room temperature, the absorption

probabilities of recoil-free fractions of Fe-ions are the same for both  $\text{Fe}^{2+}$  and  $\text{Fe}^{3+}$  (Bancroft, 1973, p. 197). This assumption only applies as a first approximation, because  $\text{Fe}^{2+}$  exhibits a lower recoil-free fraction than  $\text{Fe}^{3+}$ , but the error is generally small. The  $\text{Fe}^{3+}/\Sigma\text{Fe}$  is 0.866 to 0.946, with the exception of Shadwell 1, which has a value of 0.534. The mean  $\text{Fe}^{3+}/\Sigma\text{Fe}$  value for the Upnor Formation is  $0.88 \pm 0.02$ , while for the LMB the mean value is  $0.90 \pm 0.04$ . The mean  $\text{Fe}^{2+}$  value is  $0.18 \pm 0.03$  for the Upnor Formation, and  $0.17 \pm 0.01$  for the LMB.

#### *Glaucony chemistry*

All analyses of unweathered material lie within the defined range for glauconite (Bailey, 1980) and glauconite-smectite. Figs. 6-7 show clusters of data points for the Thanet Sand Formation and the Upnor Formation/LMB samples. The Thanet glaucony is characterised by lower Fe, and higher octahedral Al than the Upnor and LMB glaucony. The cross-plot of  $\Sigma\text{Fe}$  ions versus octahedral Al shows the expected overall inverse correlation resulting from substitution of Fe for Al in the 2:1 clay structure during glauconite formation (Fig. 7). Circled data points in Figs. 6-7 are samples from T404 Upnor Formation that have undergone slight oxidation (this core was cut

~10 years before the others) resulting in higher  $\Sigma\text{Fe}$  oxide values (Fig. 7). There is no correlation between glaucony abundance and glaucony maturity as represented by  $\text{K}^+$  content (Fig. 8). At Abbey Mills, an increase in  $\text{K}^+$  correlates with a decrease in tetrahedral Al substitution (layer charge) from the base to the top of the Upnor Formation (deposited data EDS). In T404 the tetrahedral charge is higher throughout than at any other sample location and the proportion of octahedral Fe increases up the section, from the least weathered (or possibly unweathered) base, to the interval immediately beneath the Reading Beds with disaggregated and oxidised glaucony (deposited data EDS).

Analyses of the Upnor Formation performed using ICP-OES (Deposited data ICP) have consistently higher Fe, Ti and Ca contents than those made using EDS (Deposited data EDS). This may be attributed to the presence of iron oxides (principally goethite) in the magnetically separated fraction used for the ICP-OES analyses, plus small amounts of contamination in the form of goethite-coated quartz and iron oxide-coated bioclastic debris, plus magnetic FeTi oxides. The EDS analyses are therefore believed to be closer to the true glaucony compositions, even though they are based on a much smaller amount of material. No significant differences in major element chemistry were detected between the

unweathered glaucony in the LMB and the Upnor Formation (deposited data EDS).

Most LMB and Upnor Formation samples show enrichment in light REE enrichment and heavy REE depletion in shale-normalised plots (s/n LREE, s/n HREE, respectively). (Deposited data ICP, Fig. 9).

There are no trends between REE distributions and the percentage of glauconite layers in the glaucony. One sample (Victoria Embankment 2) was magnetically separated into dark green (more mature) and olive green (less mature) pellets prior to analysis. The two profiles are similar, though the dark green granules have slightly higher LREE than the olive green granules.

In most Upnor Formation samples the s/n LREE have plateau-like profiles and broadly similar abundances although many display a slight, positive Ce anomaly ( $Ce_{anom} = 1.04 - 1.50$ ); the s/n REE steadily decrease towards the HREE (Fig. 9a-d). A few samples display a negative (i.e. a calculated ratio  $<1$ ) europium anomaly ( $Eu_{anom}$ ) of up to 0.61. The anomaly is most evident in two samples collected from Herne Bay at 0.05m and 1.50m above the base of the Upnor Formation, but it is also clearly evident in Vauxhall A1, and more subtly present ( $Eu_{anom} < 0.93$ ) in samples Shadwell 5 and 6, sample D from Herne Bay, Abbey Mills 32.5 m, Tower Bridge 1 and T404 40.3 m and 40.8 m (deposited data ICP). For the LMB and

Upnor Formation samples as a whole, there is no apparent correlation between the magnitude of the Ce anomaly and the Eu anomaly.. The Thanet glaucony separates (Fig 9e) display a sub-horizontal shale normalised REE profile. This we interpret as indicating that this glaucony contains a relatively high detrital clay content (McLennan, 1989; Jeans et al., 2000).

The  $\text{Fe}^{2+}/\Sigma\text{Fe}$  values determined by Mössbauer analysis (Fig. 10) and the EDS data were used to calculate the  $\text{Fe}^{2+}$  and  $\text{Fe}^{3+}$  contents, and hence the average structural formulae for the glaucony at each location (deposited data EDS). Where Mössbauer data was not available a value of 0.1 was assumed for  $\text{Fe}^{2+}/\Sigma\text{Fe}$ . Measured layer charge in the tetrahedral sheet is -0.17 to -0.49, and in the octahedral sheet it is -0.48 to -0.57, giving a total layer charge of -0.65 to -0.83 (deposited data EDS). There is a positive correlation between octahedral charge and  $\text{K}^+$  (Fig. 11a). There is no correlation between  $\text{K}^+$  and either  $\text{Fe}^{2+}$  or  $\text{Fe}^{3+}$ , as was also found by Rousset et al. (2004) and Odin & Matter (1981) for glauconite in general. There may be a correlation between tetrahedral charge (tetrahedral  $\text{Al}^{3+}$ ) and  $\text{K}^+$ , but it is not clear (Fig. 11b).

### *Stable isotope data*

Glaucony granule  $\delta^{18}\text{O}$  ranges from +16.1 to +20.1‰ (deposited data EDS), with an average of  $+17.8 \pm 1\%$  (n = 29) (deposited data EDS). There are no clear lateral trends in glaucony  $\delta^{18}\text{O}$  across the study area, and the only vertical trend noted is a shift to lower  $\delta^{18}\text{O}$  in the weathered interval at the top of borehole T404 (deposited data EDS), and the Thanet Formation sample also from T404. Glaucony  $\delta^2\text{H}$  ranges from -137 to -108‰, and averages  $-117 \pm 8\%$  (n = 18) (deposited data EDS); no data are available for samples from borehole T404. Tooth enameloid phosphate from five shark species from the Herne Bay Beltinge Fish Bed has  $\delta^{18}\text{O}$  ranging from +19.0 to +21.5‰ with an average of  $+19.8 \pm 1\%$  (Table 1). The most  $^{18}\text{O}$ -rich sample was obtained for a *Myliobatis* species (eagle ray) (Table 1). Oyster shell carbonate from the Abbey Mills shaft at 30.5 m has  $\delta^{18}\text{O}$  and  $\delta^{13}\text{C}$  of +25.4‰ and -1.7‰, respectively (Table 1).

### *Glaucony weathering*

Transects across a large number of seemingly unweathered grains (Fig. 12), indicate that the majority have a uniform composition from margin to core, with slightly lower analytical totals at the margin than the core, indicative of hydration linked to weathering (Table 2).

Partially altered granules from mottled Upnor Formation have opaque brown cores (owing to the presence of goethite), and olive green rims. In the more intensely altered LMB former glaucony granules are discernable as “ghost” outlines in the sediment (Fig. 13a), frequently with opaque brown cores, again owing to the presence of goethite. There are no significant chemical spatial patterns for the majority of weathered granules. Si, Al and Fe may increase or decrease between the margin and the core, depending on whether gibbsite (site 1, Table 3) or goethite has replaced the glaucony (site 2, Table 3). In BSEM images the cores of moderately weathered glaucony grains appear darker than the rims (Fig. 13b), owing to increased hydration, indicated by the lower analytical totals, and lower Fe content. (e.g. site 1 in Table 3). XRD analysis indicates that weathered granules are principally smectite-rich, mixed layer glauconite-smectite, and that small amounts of goethite and/or gibbsite are present. In the most intensely altered LMB samples, small amounts of kaolinite were detected by XRD. In BSEM images of intensely pedogenically modified clay from the LMB, clusters of goethite crystallites within the former granules are observable (Fig. 13c) and in some granules they are clustered at the core. Chemical analyses across these former granules show much higher Fe content than the slightly weathered glaucony (Table 2), owing to the

presence of goethite. Other altered granules, often in the same sample as goethite-rich ones, have very high Al contents, consistent with replacement of the glaucony by gibbsite.

## DISCUSSION

### *Glaucony chemistry*

Comparing only like with like (i.e. EDS with EDS and ICP-OES with ICP-OES), the glauconitic clay chemistry (Tables 1 & 3) shows a compositional range similar to published data for glaucony from marine transgressive sediments (e.g. Huggett & Gale, 1997; Hesselbo & Huggett, 2001; Rousset et al, 2004). The EDS and ICP-OES data show moderately good correlation, considering that the former is single point measurements, the latter is bulk glaucony data, and includes other Fe- or K-bearing minerals that may be present in the granules (Fig. 14). The two distinct groupings shown in Figs. 6-7, reflect real chemical differences, between the Thanet and Upnor/LMB glaucony, while the higher Fe content of T404 samples is almost certainly due to slight oxidation. The more variable K<sup>+</sup> and Fe in the Thanet Sand Formation samples (Fig. 6) arise from the presence of nascent glaucony granules, rich in smectite, in addition

to evolved granules.

Variations in the abundance of REEs is inferred to reflect the chemistry of the environment in which the glaucony was formed and the presence of discrete mineral phases contained within the glaucony pellets, especially REE-rich phosphate inclusions (Tóth et al., 2010). The majority of glaucony grains from the Upnor Formation have a s/n REE profile similar to Tóth et al.'s phosphate-enriched glaucony, showing enrichment in LREE and a slight positive Ce anomaly. The Herne Bay samples have the highest s/n LREE, and also marginally higher phosphate content (deposited data ICP), tentatively supporting the proposal that the variation is indeed due to cryptocrystalline REE-rich phosphates such as apatite.

Detrital shales have a relatively constant REE composition and hence using shale normalisation tends to highlight anomalies from a 'typical' shale composition more readily than, for example, chondrite normalisation (e.g. Jarvis and Jarvis, 1985; McLennan, 1989; Jeans et al., 2000). The presence of a negative Eu anomaly in fine sediments, invariably accompanied by an atypical s/n REE profile, has been used previously to infer a volcanic contribution to a sediment (Wray, 1995; Wray & Wood, 1998; Wray, 1999; Jeans et al., 2000). This is based on the observation that Eu is lost from silicate melts because of its substitution for Ca in mineral structures

of early-formed minerals, most notably plagioclase feldspars. Evolved volcanic rocks are therefore typically depleted of Eu and this depletion is preserved in sediments that incorporate volcanic debris, giving rise to  $Eu_{anom}$  lower than  $\sim 0.9$ . The negative Eu anomaly in samples collected from a range of locations of similar age implies a widespread (but not predominant) contribution of volcanic material to the depositional setting of the Upnor Formation. This detritus was most probably transported and deposited in the form of volcanic ash. From the samples currently available it is difficult to establish the frequency of volcanic events but the samples collected from Herne Bay would seem to record at least two episodes. Evidence of volcanic activity has also been recorded in the overlying sediments of the Oldhaven Beds at Herne Bay and elsewhere within the London Basin (Knox, 1983), most probably derived from volcanism to the NW of the British Isles (Ritchie & Hitchen, 1996).

The  $Fe^{3+}/\Sigma Fe$  ratios of the glaucony, the majority of which range from 0.85 to 0.90, are similar to those reported in the literature for glauconite (Odom, 1976; Fanning et al., 1989; Huggett & Cuadros, 2010). Shadwell 1 contains a small amount of siderite in the clay matrix that may have been extracted with the glaucony during magnetic separation, thereby contaminating the glaucony and reduced the calculated ratio. The  $Fe^{3+}$  in cis-M2 positions in the

lattice with moderate line-widths (0.158 – 0.280mm/s) of their spectra suggests a lack of expanding layers. The lack of expandable layers (smectite) is consistent with the XRD estimates of % swelling layers in Upnor glaucony.

#### *Weathering of glaucony*

The presence of green, unweathered glaucony granules in the goethite-containing, smectitic matrix of mottled intervals of the Upnor Formation and in the LMB suggests that glauconite can persist metastably in a weathering environment. With increasing exposure to weathering the granules change colour from green to olive to brown, as goethite and smectite replace glauconite. The weathering process removes K and Fe from the glauconite structure, and glauconite layers are replaced by smectite layers. In some instances increased weathering results in complete breakdown of the aluminosilicate structure and formation of goethite (Fig. 5c). The kaolinite detected in some samples (Fig. 5c) may also be an alteration product. Some granules, however, lose iron and preferentially alter to gibbsite rather than goethite. In the LMB weathering appears not to have been sufficiently intense to result in granules comprising only of oxides and kaolinite, as has been reported elsewhere (Courbe et al, 1981; Huggett & Gale, 1998). These findings are consistent with those of Courbe et al. (1981) who proposed a weathering sequence from

glaucinite to nontronite (iron-rich smectite) to oxides plus kaolinite. Even in the most weathered granules of the LMB some K remained, which is presumed to be in residual glauconite interlayers in glauconite-smectite. The alteration of individual granules is most intense at the granule cores, suggesting that the cores are less evolved. Less evolved glaucony is more prone to alteration (Huggett & Gale, 1997).

#### *Environment of formation*

Glauconitic minerals have been described from various settings, mostly from outer shelf and slope environments, where sedimentation rates are low (e.g. Odin & Fullager, 1988; Amorosi, 1997; Hesselbo & Huggett, 2001). The chemical and textural maturity of glaucony predominantly reflects the residence time of the granules on the seabed before burial (Odin & Matter, 1981; Amorosi, 1997; Huggett & Gale, 1997 & 1998). The more variable and overall lower degree of evolution (maturity) of the Thanet Sand Formation glaucony compared with the Upnor Formation glaucony suggests that the rate of sedimentation of the Thanet was greater than that of the Upnor, and that the Upnor glaucony is unlikely to be derived from the Thanet Sand Formation. Because nascent granules survived the granule extraction process, we discount the possibility that immature

Thanet glaucony granules were broken down and dispersed during reworking, with only the more mature granules being re-deposited in the Upnor Formation. This interpretation is consistent with the Upnor Formation glaucony having formed in an area of low energy with a low depositional rate, within a shallow marine/brackish facies, and subsequently, perhaps as a result of a major storm, having been reworked. The absence of a correlation between glaucony abundance and maturity (Fig. 8) is also consistent with an absence of intense reworking.

Glauconite formation takes place during slow sediment deposition at the sediment-water interface, with faecal pellets being the most common substrate. This is probably because the process of glauconitisation is facilitated by the presence of reactive organic matter and microbes in the faecal pellets. In recent years there have been an increasing number of reports of glaucony from shallow marine (Huggett & Gale, 1997), lagoonal and estuarine (El Albani et al., 2005), and even lacustrine (Huggett & Cuadros, 2010) environments. To these examples we now add the Upnor Formation glaucony, formed in brackish to marine water <30 m (King, 2012). From the above, it is evident that water depth *per se* is not a criterion for glaucony formation. Temperature may be a factor, in that it may control microbial pathways and rates of reaction. The water

temperature during this time interval, immediately before and during the PETM, would have been higher (equivalent to tropical) than normal for the latitude (Sluijs et al., 2006; Zacke et al., 2009; Zachos et al., 2010; Kemp et al., 2016). We are aware of no record of *shallow*, tropical/warm water glaucony, with the majority having formed at higher latitudes (McRae, 1972; Hillier, 1995; Huggett & Gale, 1997; El Albani et al., 2005; Huggett et al., 2010) or from tropical ocean water >~50m deep (e.g. Odin, 1988, Wiewióra et al., 2001).

The abundance and species of shark teeth sampled from the Herne Bay Beltinge Fish Bed at the base of the Upnor Formation represent an assemblage typical of fully marine, pelagic, warm to tropical waters (Compagno, 2001; Zacke et al., 2009). The Upnor Formation glaucony may therefore be a rare example of warm water glauconitisation. The oxygen isotopic compositions of the shark teeth provide an opportunity to estimate the temperature of the North Sea at this time. Because of its fluorapatite chemistry, large crystallite size and low organic content relative to other forms of bioapatite, shark tooth enameloid is very resistant to *post-mortem* and diagenetic alteration, and hence preserves primary oxygen isotopic compositions (Kohn & Cerling, 2002; Fischer et al., 2013). North Sea water at the time of Beltinge Fish Bed deposition and coeval

accumulation of shark teeth had an estimated oxygen isotopic composition ( $\delta^{18}\text{O}_w$ ) of  $-1.5\text{‰}$ , somewhat lower than the current value of  $-0.4$  to  $+0.4\text{‰}$  (Harwood et al., 2008). The slight depletion of  $^{18}\text{O}$  relative to modern times in part arose because of enhanced freshening from uplifted land areas and in part because of lower continental ice volume during this warm period of Earth history (Schmitz & Andreason, 2001; Zacke et al., 2009). Using this  $\delta^{18}\text{O}_w$  and the enameloid  $\delta^{18}\text{O}$  (excluding the eagle ray sample), an average water temperature of  $23.5\pm 2^\circ\text{C}$  can be calculated from the bioapatite phosphate-water oxygen isotope geothermometer of Lécuyer et al. (2013). The average temperature decreases to  $21.5^\circ\text{C}$  if the eagle ray sample is included. These temperatures correspond well with the ranges ( $19\text{-}23^\circ\text{C}$ ,  $\delta^{18}\text{O}_w = -1.5\text{‰}$ ;  $21\text{-}24^\circ\text{C}$ ,  $\delta^{18}\text{O}_w = -1.0\text{‰}$ ) previously proposed for the region using shark tooth  $\delta^{18}\text{O}$  from the Late Thanetian to Early Ypresian (Zacke et al., 2009). This time interval includes the depositional period of the Upnor Formation.

Accordingly, we have considered the oxygen and hydrogen isotopic data obtained for the glaucony within the context of a warm water regime, set at  $23\pm 3^\circ\text{C}$ , based on shark tooth  $\delta^{18}\text{O}$ , as described above. This is a conservative temperature estimate, given that this already warm time period (Zachos et al., 2001) experienced a further upward spike in temperature, the PETM, towards the end of

deposition of the Upnor Formation at ~56.0-55.7 Ma (Westerhold et al., 2009; Charles et al., 2011), during which even higher temperatures and greater freshening of the North Sea likely occurred (Zacke et al., 2009).

The illite-water oxygen isotope geothermometer of Sheppard & Gilg (1996) is used here to interpret the glaucony  $\delta^{18}\text{O}$ , given its close consistency with the glauconite-water oxygen isotope fractionation factor reported by Savin & Epstein (1970). For the range of glaucony oxygen isotopic compositions, values of  $\delta^{18}\text{O}_w$  calculated for 20-26°C are all substantially lower (-8.1 to -3.0‰) than the Late Thanetian to Early Ypresian North Sea estimate of -1.5‰. For the glaucony  $\delta^{18}\text{O}$  (+18.8‰) obtained for the basal bed of the Upnor Formation at Herne Bay (Beltinge Fish Bed), for example,  $\delta^{18}\text{O}_w$  ranges from -5.4 to -4.3‰. Using the average glaucony  $\delta^{18}\text{O}$  (+17.8‰) for the full stratigraphic range of the Upnor Formation, the range of  $\delta^{18}\text{O}_w$  is -6.4 to -5.3‰. The oyster shell  $\delta^{18}\text{O}$  for the Abbey Mills 30.5 m sample yields  $\delta^{18}\text{O}_w = -4.4$  to  $-3.1$ ‰ for  $23 \pm 3^\circ\text{C}$ , only slightly higher than glaucony for the same stratigraphic position ( $\delta^{18}\text{O}_w = -5.2$  to  $-4.1$ ‰). The  $\delta^{13}\text{C}$  of this oyster shell (-1.7‰) is consistent with the major negative shift (by 2 to 4‰) in marine foraminifera associated with the PETM reported by Kennett & Stott (1991). Lower oyster shell  $\delta^{13}\text{C}$  in the Upnor Formation could also simply indicate a greater

contribution from  $^{13}\text{C}$ -depleted sources of dissolved inorganic carbon in an estuarine depositional environment.

The presence of a significant fraction of meteoric water during glaucony formation is further confirmed by its hydrogen isotopic composition. Using the glauconite-water hydrogen isotopic fractionation factor of Savin & Epstein (1970),  $\delta^2\text{H}_w$  is  $-68$  to  $-37\text{‰}$  with an average of  $-46\text{‰}$ . Using the illite-smectite hydrogen isotope geothermometer of Capuano (1992), even lower average  $\delta^2\text{H}_w$  ( $-66$  to  $-63\text{‰}$ ) can be calculated for  $23\pm 3^\circ\text{C}$ . Such low hydrogen isotopic compositions require a significant fraction of meteoric water in the environment during glaucony formation.

In summary, the oxygen and/or hydrogen isotopic compositions obtained for the glaucony and oyster shell are characteristic of significant freshwater input (Craig, 1961). The range in calculated water isotopic compositions may reflect in part variation in water temperature during the depositional history of the Upnor Formation, and/or even more likely, variations in the relative fractions (and  $\delta$ -values) of fresh- and sea-water end-members that mixed within this estuarine environment. This finding is wholly consistent with the sedimentological interpretation of a shallow marine to estuarine environment for the Upnor Formation (King, 2012, and references

therein), particularly during a time of enhanced outflow of meteoric water.

It follows from the shallow, brackish environment of deposition suggested by the sedimentary and isotopic data, that the glaucony formed in warm (~21-23°C), shallow and brackish water. *In situ* glaucony is typically associated with outer shelf sediments, where the water temperature is ~10°C. The Upnor glaucony is apparently closer in temperature of formation and environment of deposition to verdine, which is associated with tropical seas, typically forming offshore from major river systems (Odin et al. 1988; Odin & Sen Gupta, 1988; Huggett et al. 2015). There is not, therefore, a clear distinction between the environmental requirements of verdine (or odinite) and glaucony (or glauconite).

## CONCLUSIONS

The Upnor Formation glaucony is evolved, indicating a residence time at, or very close to, the sediment-water interface of around  $10^5$  years, assuming that the elevated temperature did not increase the rate of glauconitisation. For this to have occurred in a shallow marine/estuarine environment, the glaucony must have formed in an

area of low energy with a low depositional rate, and subsequently, perhaps as a result of major storm, been reworked. Many of the granules are well rounded, and this may be in part result from abrasive reworking, as fragments of granules are also present. None of the techniques applied in this study permit unequivocal determination of the quantitative importance of reworking of glaucony in the Upnor Formation. The REE profiles indicate a range of parent materials, including igneous rock, probably volcanic ash, for the glaucony. Shark tooth  $\delta^{18}\text{O}$  from the basal Beltinge Fish Bed of the Upnor Formations suggests marine water temperatures of  $\sim 23 \pm 3^\circ\text{C}$ . Assuming a similar range of temperature for glaucony formation, its  $\delta^{18}\text{O}$  and  $\delta^2\text{H}$  require formation from brackish water (i.e., isotopic compositions significantly lower than open marine water). The variation in glaucony  $\delta^{18}\text{O}$  ( $\pm 2\text{‰}$ ) and  $\delta^2\text{H}$  ( $\pm 10\text{‰}$ ) is consistent with deposition in a shallow marine/estuarine environment, in which variable water isotopic compositions would accompany salinity fluctuations arising from mixing of marine and fresh water. The less evolved Thanet Sand Formation glaucony, and the paucity of glaucony in this, the oldest of the formations studied here, are consistent with *in situ* glaucony precipitation in the Upnor Formation, rather than with precipitation in the fully marine Thanet Sand Formation and subsequent reworking into the Upnor Formation. The

absence of any correlation between glaucony maturity and abundance also implies an absence of significant winnowing. Formation of the Upnor glaucony in brackish, shallow waters suggests that there is not a clear distinction between the environmental requirements of verdine (or odinite) and glaucony (or glauconite). Factors other than temperature and salinity are therefore inferred to be responsible for whether verdine or glaucony precipitates.

### **Acknowledgements**

Thames Water (Thames Tideway Project) are thanked for providing the London borehole samples. The staff of the Natural History Museum Imaging and Microanalysis unit are thanked for assistance with the SEM work. Martin Gill of Imperial College is thanked for assistance with the XRD analysis and Lorna Dyer of the University of Greenwich is thanked for assistance with the ICP-OES and –MS analysis. Grace Yau, Li Huang and Kim Law of the Laboratory for Stable Isotope Science (LSIS) at the University of Western Ontario are thanked for assistance with the stable isotope analyses. Financial support for the isotopic measurements was provided by the Natural Sciences and Engineering Research Council of Canada, the Canada Foundation for Innovation and the Ontario Research Fund, and

research time for FJL was funded through the Canada Research  
Chairs program. This is LSIS contribution # 334.

## REFERENCES

- Ali, J.R. & Jolley, D.W. (1996) Chronostratigraphic framework for the Thanetian and lower Ypresian deposits of southern England. Pp129-140 in: *Correlation of the Early Palaeogene in Northwest Europe*. (R.W.O. Knox, R.M. Corfield, & R.E. Dunay, editors). Geological Society of London Special Publication 101, Geological Society, London.
- Amorosi, A. & Centineo, M.C. (1997) Glaucony from the Eocene of the Isle of Wight (southern UK): implications for basin analysis. *Journal of the Geological Society London*, **154**, 887–896.
- Bailey, S.W. (1980) Summary of recommendations of AIPEA nomenclature committee. *Clays and Clay Minerals* **28**, 73-78.
- Bancroft, G.M. (1973) Mössbauer spectroscopy: an Introduction for Inorganic chemists and Geochemists. McGraw Hill, London, 251pp.
- Blondeau, A. & Pomerol, C. (1968) A contribution to the sedimentological study of the Palaeogene of England. *Proceedings of the Geologists' Association* **79**, 441-455.

- Borthwick, J. & Harmon, R.S. (1982) A note regarding  $\text{ClF}_3$  as an alternative to  $\text{BrF}_5$  for oxygen isotope analysis. *Geochimica et Cosmochimica Acta* **46**, 1665-1668.
- Brindley, G.W. and Brown, G. (1980) Crystal structures of clay minerals and their X-ray identification. Mineralogical Society Monograph No. 5, Mineralogical Society, London, 495pp.
- Capuano, R.M. (1992) The temperature dependence of hydrogen isotope fractionation between clay minerals and water: Evidence from a geopressured system. *Geochimica et Cosmochimica Acta* **56**, 2547-2554.
- Charles, A.J, Condon, D.J., Harding, I.C., Pälke, H., Marshall, J.E.A, Cui, Y., Kump, L. & Croudace, I.W. (2011) Constraints on the numerical age of the Paleocene-Eocene boundary. *Geochemistry Geophysics Geosystems* **12**, 1-19.
- Clayton, R.N. & Mayeda, T.K. (1963) The use of bromine pentafluoride in the extraction of oxygen from oxides and silicates for isotopic analysis. *Geochimica et Cosmochimica Acta* **27**, 43-52.
- Compagno, L.J.V. (2001) Sharks of the World. An Annotated and Illustrated Catalogue of Shark Species Known to Date. Volume 2. Bullhead, Mackerel and Carpet Sharks

(Heterodontiformes, Lamniformes and Orectolobiformes).

FAO Species Catalogue for Fishery Purposes. Food and Agriculture Organization of the United Nations, Rome. 269pp.

Coplen, T.B. (1996) New guidelines for reporting stable hydrogen, carbon, and oxygen isotope-ratio data. *Geochimica et Cosmochimica Acta* **60**, 3359-3360.

Coplen, T.B., Brand, W.A., Gehre, M., Gröning, M., Meijer, H.A.J., Toman, B. & Verkouteren, R.M. (2006) After two decades a second anchor for the VPDB  $\delta^{13}\text{C}$  scale. *Rapid Communications in Mass Spectrometry* **20**, 3165-3166.

Courbe, C. Velde, B. & Meunier, A. (1981) Weathering of glauconites; reversal of the glauconitization process in a soil profile in western France. *Clay Minerals* **16**, 231-243.

Craig, H. (1961) Isotopic variations in meteoric waters. *Science* **133**, 1702-1703.

Drits, V.A., Dainyak, L.G., Muller, F., Besson, G., and Manceau, A. (1997) Isomorphous cation distribution in celadonites, glauconites and Fe-illites determined by Infrared, Mössbauer and EXAFS spectroscopy. *Clay Minerals* **32**, 153–180.

El Albani, A., Meunier, A. & Fürsich, F. (2005) Unusual occurrence of glauconite in a shallow lagoonal environment (Lower

Cretaceous, Northern Aquitaine Basin, SW France). *Terra Nova* **17**, 537-544.

Ellison, R.A., Ali, J.R., Hine, N.M. & Jolley, D.W. (1996)

Recognition of Chron C25n in the upper Paleocene Upnor Formation of the London Basin, UK. Pp. 185-193 in: *Correlation of the Early Palaeogene in Northwest Europe*. (R.W.O. Knox, R.M. Corfield, & R.E. Dunay, editors). Geological Society of London Special Publication 101, Geological Society, London.

Ellison, R.A., Woods, M.A., Allen, D.J., Forster, A., Pharoah, T.C. &

King, C. (2004) Geology of London; special memoir for 1:50 000 geological sheets 256 (north London, 257 (Romford), 270 (south London) and 271 (Dartford) (England and Wales) Memoir of the British Geological Survey. 114pp.

Fanning, D.S., Rabenhorst, M. C, May, L. & Wagner, D.P. (1989)

Oxidation state of iron in glauconite from oxidized and reduced zones of soil-geologic columns. *Clays and Clay Minerals*, **37**, 59-64.

Firsching, F.H. (1961) Precipitation of silver phosphate from

homogeneous solution. *Analytical Chemistry* **33**, 873–874.

Fischer, J., Schneider, J.W., Voigt, S., Joachimski, M.M.,

- Tichomirowa, M., Tütken, T., Götze, J. & Berner, U. (2013) Oxygen and strontium isotopes from fossil shark teeth: Environmental and ecological implications for Late Palaeozoic European basins. *Chemical Geology* **342**, 44-62.
- Godfrey, J.D. (1962) The deuterium content of hydrous minerals. *Geochimica et Cosmochimica Acta* **26**, 1214-1238.
- Harwood, J.P., Dennis, D.F., Marca, A.D., Pilling, G.M. & Millner, R. (2008) The oxygen isotope composition of water masses within the North Sea. *Estuarine, Coastal and Shelf Science* **78**, 353-359.
- Hesselbo, S.P. & Huggett, J.M. (2001) Glaucony in ocean-margin sequence stratigraphy (mid-Cenozoic, offshore New Jersey, USA, ODP, Leg 174A). *Journal of Sedimentary Petrology* **74**, 599-607.
- Hillier S. (1995) Erosion, sedimentation and sedimentary origin of clays. Pp. 162–219 in: *Origin and Mineralogy of Clays* (B. Velde, editor). Springer, Berlin, Heidelberg, New York.
- Hine, N.M. (1994) Calcareous nannoplankton assemblages from the Thanet Sand Formation in Bradwell Borehole, Essex, England. *GFF* **116**, 54-55.

- Huggett, J.M. & Gale, A.S. (1997) Petrology and palaeoenvironmental significance of glaucony in the Eocene succession at Whitecliff Bay, Hampshire Basin, UK. *Journal of the Geological Society* **154**, 897-912.
- Huggett, J.M. & Gale, A.S. (1998) Petrography and diagenesis of the Thames Group at Whitecliff Bay, Isle of White, UK. *Proceedings of the Geologists Association*, **109**, 99-113.
- Huggett, J.M. & Laenen, B. (1996) Green clays from the lower Oligocene of Aardebrug, Belgium, A re-evaluation. *Clay Minerals* **31**, 557-562.
- Huggett, J.M & Cuadros, J. (2010) Glauconite formation in lacustrine/palaeosol sediments, Isle of Wight (Hampshire basin), UK, *Clay Minerals* **45**, 35-50.
- Huggett, J.M., Gale, A.S. & McCarty, D. (2010) Petrology and Palaeoenvironmental significance of authigenic iron-rich clays, carbonates and apatite in the Claiborne Group, Middle Eocene, NE Texas. *Sedimentary Geology* **228**, 119-139.
- Huggett, J.M., Burley, S.D., Longstaffe, F.J, Saha, S. & Oates, M. . (2015) The nature and origin of authigenic chlorite and related cements in Oligo-Miocene reservoir sandstones, Tapti gas fields, Surat Depression, Offshore Western India. *Journal of*

*Petroleum Geology* **38**, 383-409.

Jarvis, I. & Jarvis, K.E. (1985) Rare-earth element geochemistry of standard sediments: a study using inductively coupled plasma spectrometry. *Chemical Geology* **53**, 335-344.

Jeans, C.V., Wray, D.S., Merriman, R.J. & Fisher, M.J. (2000) Volcanogenic clays in Jurassic and Cretaceous strata of England and the North Sea basin. *Clay Minerals* **35**, 25-55.

Kelly, J.C. & Webb, J.A. (1999) The genesis of glaucony in the Oligo–Miocene Torquay Group, southeastern Australia: petrographic and geochemical evidence. *Sedimentary Geology* **125**, 99-114.

Kemp, S.J., Ellis, M.A., Mountney, I. & Kender, S. (2016) Palaeoclimatic implications of high resolution clay mineral assemblages preceding and across the onset of the Palaeocene–Eocene Thermal Maximum, North Sea Basin. *Clay Minerals*, **51**, 793–813

Kennett, J.P. & Stott, L.D. (1991) Abrupt deep-sea warming, palaeoceanographic changes and benthic extinctions at the end of the Palaeocene. *Nature* **353**, 225-229.

King, C. (2012) The Stratigraphical framework for the Palaeogene successions of the London Basin, UK. British Geological

Survey open report OR/12/004, 94pp.

King, C. (2016) A revised correlation of Tertiary rocks in the British Isles and adjacent areas of NW Europe. Geological Society Special Report Number 27, 719pp.

Knox, R.W.O'B. (1983) Volcanic ash in the Oldhaven Beds of southeast England, and its stratigraphic significance. *Proceedings of the Geologists' Association* **94**, 245-250.

Knox, R.W.O'B. (1996) Tectonic controls on sequence development in the Palaeocene and earliest Eocene of southeast England: implications for North Sea stratigraphy. Pp. 209-230 in *Sequence Stratigraphy in British Geology* (S.P. Hesselbo & D.N. Parkinson, editors). Geological Society Special Publication 103, Geological Society, London.

Kohn, M.J. & Cerling, T.E. (2002) Stable isotope compositions of biological apatite. Pp. 455-488 in: *Phosphates. Geochemical, Geobiological, and Materials Importance*. (M.J. Kohn, J. Rakovan, & J.M. Hughes, editors). Mineralogical Society of America, *Reviews in Mineralogy and Geochemistry* **48**,

Kyser, T.K. & O'Neil, J.R. (1984) Hydrogen isotope systematics of submarine basalts. *Geochimica et Cosmochimica Acta* **48**, 2123-2133.

- Lagarec, K. & Rancourt, G.K. (1998) Mössbauer Spectral Analysis Software, Mössbauer Group Physics department, University of Ottawa, Canada.
- Lécuyer, C., Amiot, R., Touzeau, A. & Trotter, J. (2013) Calibration of the phosphate  $\delta^{18}\text{O}$  thermometer with carbonate-water isotope fractionation equations. *Chemical Geology* **347**, 217-226.
- McLennan, S.M. (1989) Rare earth elements in sedimentary rocks: influence of provenance and sedimentary processes. Pp. 169-200 in: *Geochemistry and Mineralogy of the Rare Earth Elements* (B. R. Lipin & G. A. McKay, editors). Mineralogical Society of America, Reviews in Mineralogy 21, Chantilly, Virginia, USA.
- McRae, S.G. (1972) Glauconite. *Earth Science Reviews* **8**, 397-440.
- Moore, D.M. & Reynolds, R.C. Jr. (1989) X-ray Diffraction and the Identification and Analysis of Clay Minerals. Oxford University Press, New York. 332pp.
- Morton, A.C. (1982) The provenance and diagenesis of Palaeogene sandstones of southeast England as indicated by heavy mineral analysis. *Proceedings of the Geologist's Association*, **93**, 263-274.
- Newman, T. (2013) Causes of confined space hypoxia during

underground construction in the Lambeth Group beneath London. PhD thesis, University of London. 173pp.

- Odom, E. (1976) Microstructure, mineralogy and chemistry of Cambrian glauconite pellets and glauconite, central USA, *Clays and Clay Minerals* **24**, 232-238.
- Odin, G.S. & Fullager, P.D. (1988) Geological significance of the glaucony facies. Pp. 295-332 in: *Green Marine Clays* (Odin, G.S. (editor). Developments in Sedimentology 45. Elsevier, Amsterdam.
- Odin, G.S. & Matter, A. (1981) De glauconiarum origine. *Sedimentology* **28**, 611-641.
- Odin, G.S. & Stephan, J.F. (1981) The Occurrence of deep-water glaucony from the Eastern Pacific: the result of in situ genesis or subsidence? Pp. 419-428 in: Initial Reports of the Deep Sea Drilling Project, V. LXVI, (Watkins, J.S. & Moore, J.C., editors). US Government Printing Office, Washington D.C., USA.
- Odin, G.S., (1988) Glaucony from the Gulf of Guinea. Pp. 225-247 in: *Green Marine Clays*. (G.S. Odin, editor), Developments in Sedimentology, 45. Elsevier, Amsterdam.

Odin, G.S., Debenay, J.P. & Masse, J.P. (1988) The verdine facies deposits identified in 1988. Pp. 131-159 in: *Green Marine Clays*. (G.S. Odin, editor), Developments in Sedimentology, 45. Elsevier, Amsterdam.

Odin, G.S. & Sen Gupta, B.K. (1988) The geological significance of the verdine facies. Pp. 205-247 in: *Green Marine Clays*. (G.S. Odin, editor). Developments in Sedimentology, 45. Elsevier, Amsterdam.

Powell, J.A., Brinkhuis, H. & Bujak, J.P. (1996) Upper Palaeocene-Lower Eocene dinoflagellate cyst sequence biostratigraphy of south east England. Pp. 145-183 in: *Correlation of the Early Palaeogene in Northwest Europe*. (R.W.O. Knox, R.M. Corfield, & R.E. Dunay, editors). Geological Society of London Special Publication 101, Geological Society, London.

Ritchie, J.D. & Hitchen, K. (1996) Early Paleogene offshore igneous activity to the northwest of the UK and its relationship to the North Atlantic Igneous Province. Pp. 63-78 in: *Correlation of the Early Palaeogene in Northwest Europe*. (R.W.O. Knox, R.M. Corfield, & R.E. Dunay, editors). Geological Society of London Special Publication 101, Geological Society, London.

- Rousset, D., Leclerc, S., Clauer, N., Lancelot, J. Cathelineau, M. & Aranyosy, J-F. (2004) Age and Origin of Albian Glauconites and Associated Clay Minerals Inferred from a Detailed Geochemical Analysis. *Journal of Sedimentary Research*, **74**, 631-642.
- Savin, S.M. & Epstein, S. (1970) The oxygen and hydrogen isotope geochemistry of clay minerals. *Geochimica et Cosmochimica Acta* **34**, p. 25-42.
- Schmidt, B. & Andreason, F.P. (2001) Air humidity and lake  $\delta^{18}\text{O}$  during the latest Paleocene–earliest Eocene in France from recent and fossil fresh-water and marine gastropod  $\delta^{18}\text{O}$ ,  $\delta^{13}\text{C}$ , and  $^{87}\text{Sr}/^{86}\text{Sr}$ . *Geological Society of America Bulletin* **113**, 774–789.
- Sheppard, S.M.F. & Gilg, H.A (1996) Stable isotope geochemistry of clay minerals. *Clay Minerals* **31**, 1-24.
- Skipper, J.A. (1999) The stratigraphy of the Lambeth Group (Paleocene) of South East England. PhD thesis, Imperial College London. 297pp.
- Sluijs, A., Schouten, S., Pagani, M., Woltering, M., Brinkhuis, H., Jaap, S., Damsté, J.S., Dickens, Huber, M. Reichart, J-G., Ruediger, S., Mathiessen, J., Lourens, L.J. Pedentchouk,

Backman, J., Moran, K. and the Expedition 302 Scientists (2006). Subtropical Arctic Ocean temperatures during the Palaeocene/Eocene thermal maximum. *Nature*, **441**, 610–613.

Stuart-Williams HLQ, Schwarcz HP (1995) Oxygen isotopic analysis of silver orthophosphate using a reaction with bromine. *Geochimica et Cosmochimica Acta* **59**, 3837-3841

Tóth, E., Weiszburg, T.G., Jeffries, T.E., Williams, C.T., Bartha, A., Bertalan, E. & Cora, I. (2010). Submicroscopic accessory minerals overprinting clay mineral REE patterns (celadonite–glauconite group examples). *Chemical Geology* **269**, 312-328.

Ward, D.J. (1978) The Lower London Tertiary (Palaeocene) succession at Herne Bay, Kent. *Report of the Institute of Geological Sciences* **78/10**, 17pp.

Weir, A.H. & Catt, J.A. (1969) The mineralogy of Palaeogene sediments in Northeast Kent (Great Britain). *Sedimentary Geology* **3**, 17-33.

- Westerhold, T., Röhl, U., McCarren, H.K. & Zachos, J.C. (2009)  
Latest on the absolute age of the Paleocene–Eocene Thermal  
Maximum (PETM): New insights from exact stratigraphic  
position of key ash layers +19 and –17. *Earth and Planetary  
Science Letters* 287, 412-419.
- Wiewióra, A., Giresse, P., Petit, S. and Wilamowski, A. (2001) A  
deep-water glauconitization process on the Ivory Coast-Ghana  
marginal ridge (ODP site 959): determination of Fe<sup>3+</sup>-rich  
montmorillonite in green grains. *Clays and Clay Minerals* 49,  
540-558.
- Wray, D.S. (1995) Origin of clay-rich beds in Turonian chalks from  
Lower Saxony, Germany - a rare earth element study.  
*Chemical Geology* **119**, 161-173.
- Wray, D.S. (1999) Identification and long-range correlation of  
bentonites in Turonian - Coniacian (Upper Cretaceous) chalks  
of northwest Europe. *Geological Magazine* **136**, 361-371.
- Wray, D.S. & Wood, C.J. (1998) Distinction between detrital and  
volcanogenic clay-rich beds in Turonian-Coniacian chalks of  
eastern England. *Proceedings of the Yorkshire Geological  
Society* **52**, 95-105.

Zacke, A. Voigt, S., Joachimski, M.M., Gale, A.S., Ward, D.J. &

Tütken, T. (2009) Surface water-freshening and high-latitude river discharge in the Eocene North Sea. *Journal of the Geological Society*, **166**, 969-980.

Zachos, J., Pagani, M., Sloan, L., Thomas, E., & Billups, K. (2001)

Trends, rythms and aberrations in global climate 65 Ma to present. *Science* **292**, 686-693.

#### CAPTIONS FOR FIGURES

Fig. 1 Map of South East England showing approximate extent of the London Basin and place names mentioned in the text. HB = Herne Bay, CA = Canterbury, both in East Kent, R = Reading, Berkshire. The inset map shows the locations of the central London Localities from which samples were obtained. V = Vauxhall, AE – Albert Embankment, VE = Victoria Embankment, B = Blackfriars, TB = Tower Bridge, S = Shadwell, AM = Abbey Mills, C = Charlton.

Respectively.

Fig. 2 Simplified stratigraphy for the Thanet Sand Formation and Lambeth Group. The depositional sequences follow the interpretation by Knox (1996) of the of the early Palaeogene succession of southeast England. PETM = Paleocene-Eocene Thermal Maximum.

Fig. 3 Optical microscope images, scale bars are 100  $\mu\text{m}$ . (a) glaucony pellets from Victoria Embankment 2, mostly fragments, with internal vermiform structure (v). The olive-brown colour suggests that a small proportion of goethite is present; (b) entire glaucony pellets (g) and fragments of pellets (f) in quartz-rich sand from Blackfriars 4; (c) matrix of disaggregated glaucony granules (g) in sample Shadwell 2; (d) Green, unweathered glaucony (g) in weathered, goethite-rich matrix (m).

Fig. 4a BSEM image showing the fracturing of granules that occurs during glaucony evolution (arrows). This indicates *in situ* evolution of the granules because reworking would disperse the fragments. Scale bar = 500  $\mu\text{m}$ .

Fig. 4b BSEM image of nascent glaucony (NG) from the Thanet Sand Formation. Relict crystalline textures suggest the glaucony has replaced a volcanic rock fragment. Scale bar = 50  $\mu\text{m}$ .

Fig. 5 XRD traces; vertical scales are counts per second. (a)  $<2 \mu\text{m}$  fraction of glaucony pellets from Shadwell 1. This is a typical suite of traces for the Upnor Formation glaucony. The 1nm reflections are broad indicating poor crystallinity, or small crystallite size; (b) XRD traces for the  $<2 \mu\text{m}$  fraction of glaucony pellets from the Thanet Sand Formation, sample Shadwell 9; (c) XRD trace of magnetically separated glaucony from weathered sample Vauxhall A2. The pellets were disaggregated, and very gently ground prior to scanning.

Fig. 6 interlayer K ions/ $\text{O}_4(\text{OH})$  plotted against octahedral  $\Sigma\text{Fe}$  ions/ $\text{O}_4(\text{OH})$ . Circled data points are for the slightly oxidised T404 samples.

Fig.7 Octahedral Al ions/ $\text{O}_4(\text{OH})$  plotted against  $\Sigma\text{Fe}$  ions/ $\text{O}_4(\text{OH})$ . Data points contained within the ellipse represent the slightly oxidised T404 samples.

Fig. 8 Interlayer K ions/ $\text{O}_4(\text{OH})$  plotted against percent glaucony determined by modal analysis of thin sections.

Fig. 9 Shale normalised REE plots grouped by geographic location (for details of the normalisation procedure see the methods section).

The presence of a negative europium (Eu) anomaly is taken to indicate the presence of altered acidic volcanic ash.

Fig. 10 Room temperature Mössbauer spectra of glauconite samples from a) Shadwell 2 and (b) Abbey Mills 29 m, fitted as  $[1\text{Fe}^{2+} + 2\text{Fe}^{3+}]$  and  $[2\text{Fe}^{2+} + 1\text{Fe}^{3+}]$ .

Fig. 11(a) Interlayer K ions/ $\text{O}_4(\text{OH})$  plotted against octahedral charge.

Fig. 11(b) Interlayer K ions/ $\text{O}_4(\text{OH})$  plotted against tetrahedral charge. Data points contained within the ellipse represent the slightly oxidised T404 samples.

Fig. 12 BSEM images of unweathered glaucony pellets with analysis locations corresponding to the analyses in Table 2, sites 1-4. Scale bars =  $100\ \mu\text{m}$ .

Fig. 13 (a) Thin section image of intensely weathered glauconitic sandstone (scale bar =  $100\ \mu\text{m}$ ). The green colour of fresh glaucony is entirely gone, owing to replacement of iron-rich clay by iron oxides, plus smectite, kaolinite or gibbsite. The former pellets may be recognised from “ghost” outlines in the clay; (b) BSEM image of slightly weathered glauconite (scale bar =  $100\ \mu\text{m}$ ). The darker core indicates that Fe has been lost from this region. The bright rim is unweathered glaucony. Analysis locations corresponding to the analyses in Table 3, site 1; (c) BSEM of intensely weathered glaucony with iron oxide particles (white) concentrated in the core, implying that oxidation has been most intense there, rather than at

the margin. Analysis locations corresponding to the analyses in Table 3, site 2. Scale bar = 100  $\mu\text{m}$ .

Fig. 14 (a) K oxide as measured by EDS X-ray analysis plotted against K oxide as measured by ICP-OES. (b) Fe oxides as measured by EDS X-ray analysis plotted against Fe oxides as measured by ICP-OES

#### CAPTIONS FOR TABLES

Deposited data. Point-count, O- and H-isotope, XRD (%1 nm clay) and quantitative EDS data for glaucony from each borehole and site. Samples are listed from west (Vauxhall) to east (Herne Bay). Isotope data indicated in bold are average values of duplicate analyses. ND = analysis Not Done. Cation proportions are calculated on the basis of  $\text{O}_4(\text{OH})$ . Where values for  $\text{Fe}^{3+}$  from Mossbauer are not available, the mean  $\text{Fe}^{3+}/\Sigma\text{Fe}$  value is assumed; these values are 0.9 for the LMB Reading Formation and 0.88 for the Upnor Formation.

Deposited data—ICP, —ICP-OES, and —MS for all analysed samples.

Table 1 Stable isotope results for oyster shell and shark teeth.

Table 2 EDS X-ray analysis transects across fresh glaucony pellets, with values presented as normalised oxide weight%. For each grain spectrum 1 is from the margin of the grain and the highest number

spectrum is from the core. In some grains Al decreases and Fe increases by 1-2% between the margin and the core, but in the majority there are no significant trends. Totals increase slightly from margin to core indicating that slight hydration/hydrolysis has occurred at the margins. Normalised data allows direct comparison among analyses.

Table 3 EDS X-ray analysis transects across weathered glaucony. For each grain spectrum 1 is from the margin of the grain and the highest number spectrum is from the core. Normalised data allows direct comparison among analyses.

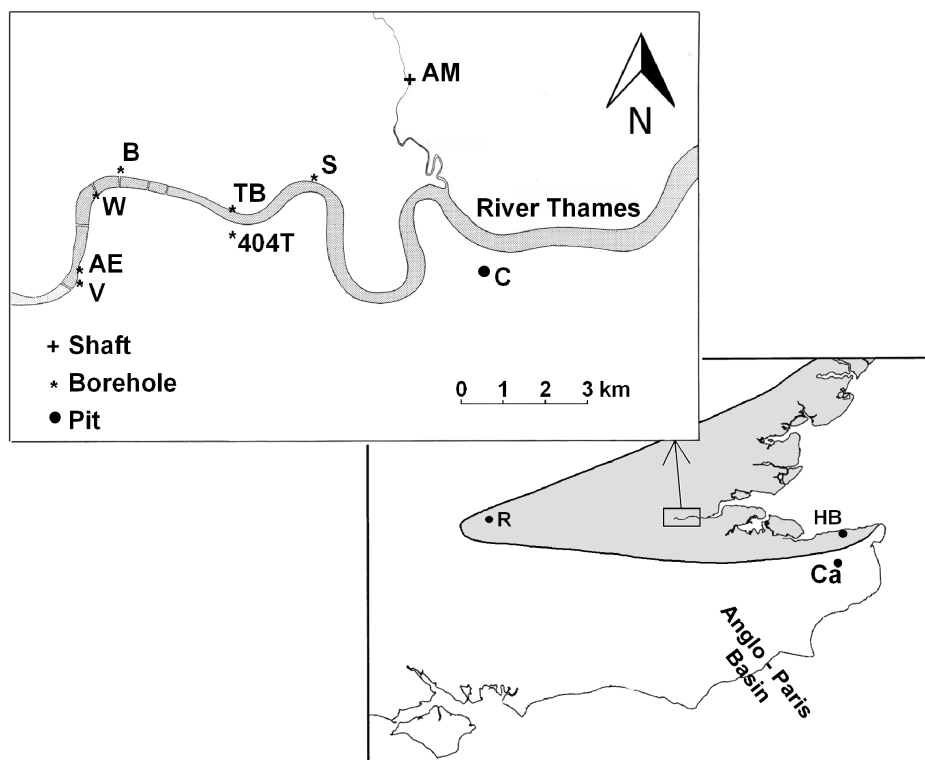


Fig. 1

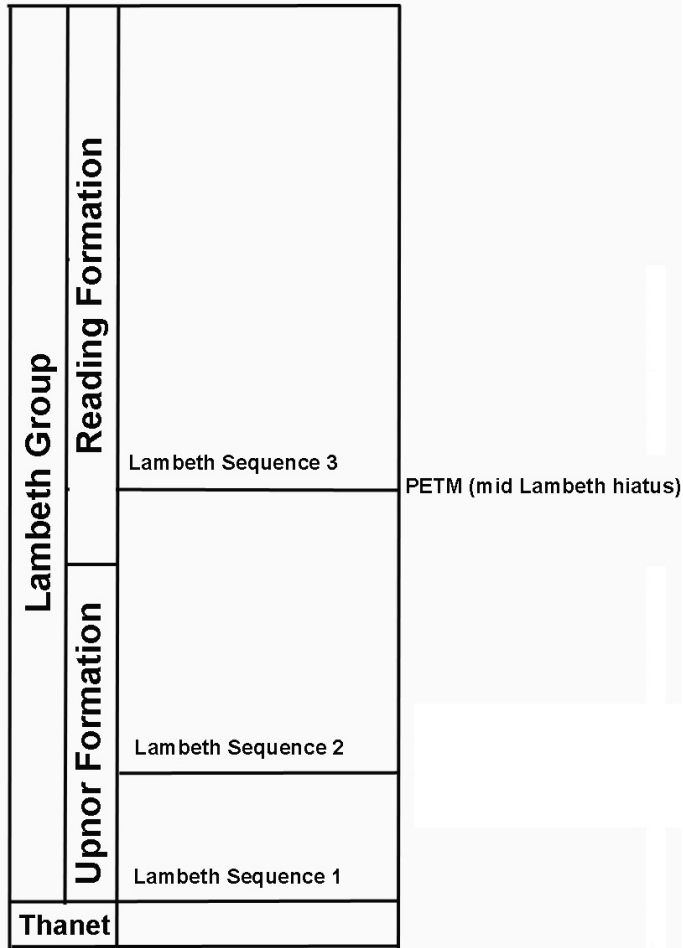
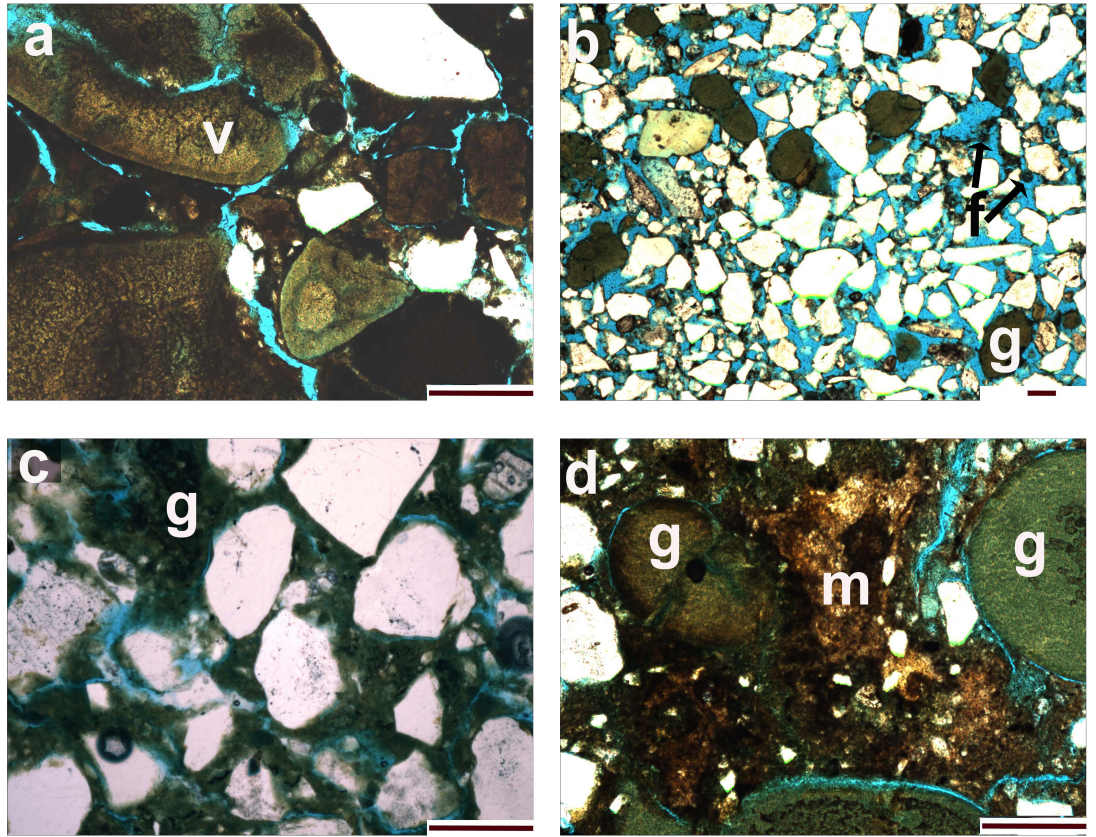


Fig 2

Fig 3



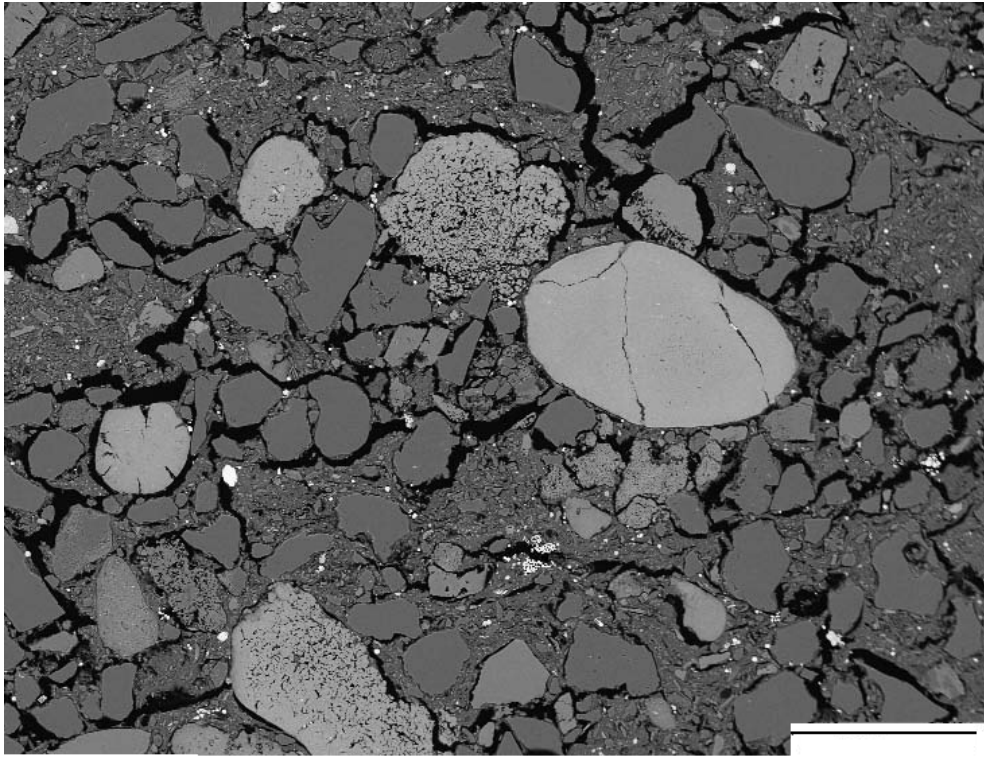


Fig. 4a

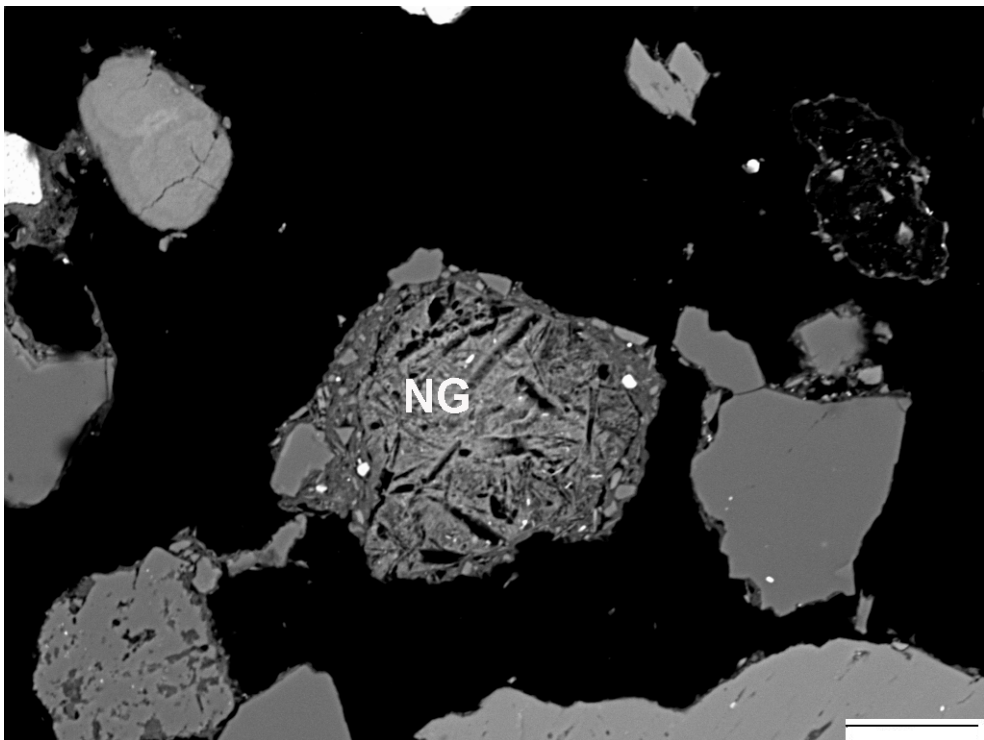


Fig. 4b

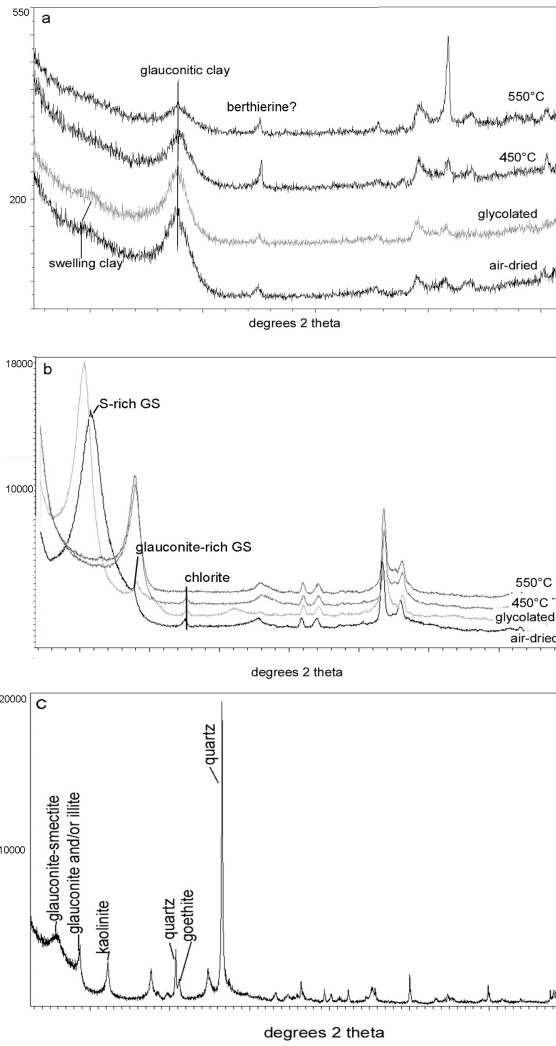


Fig 5

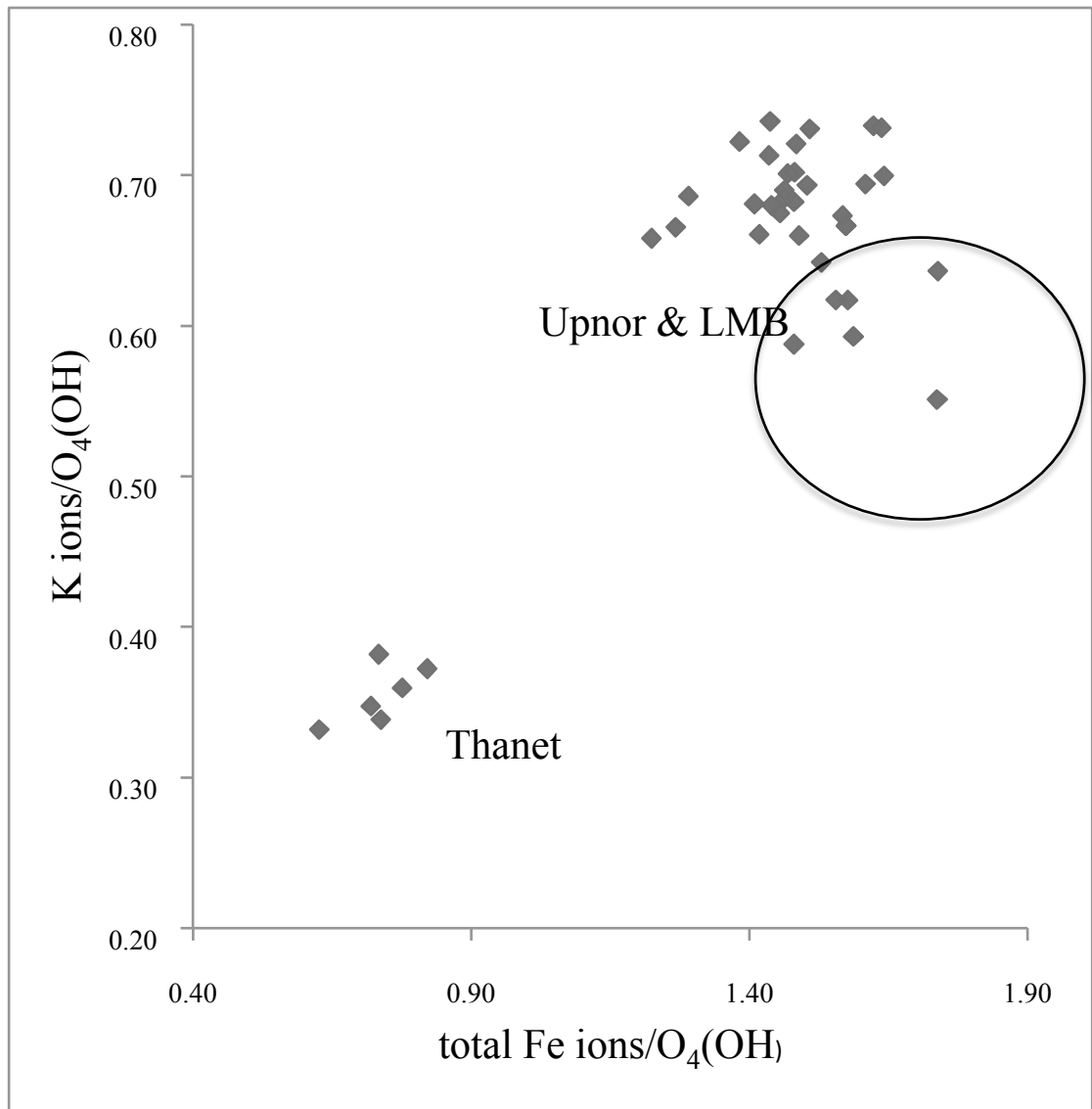


Fig 6

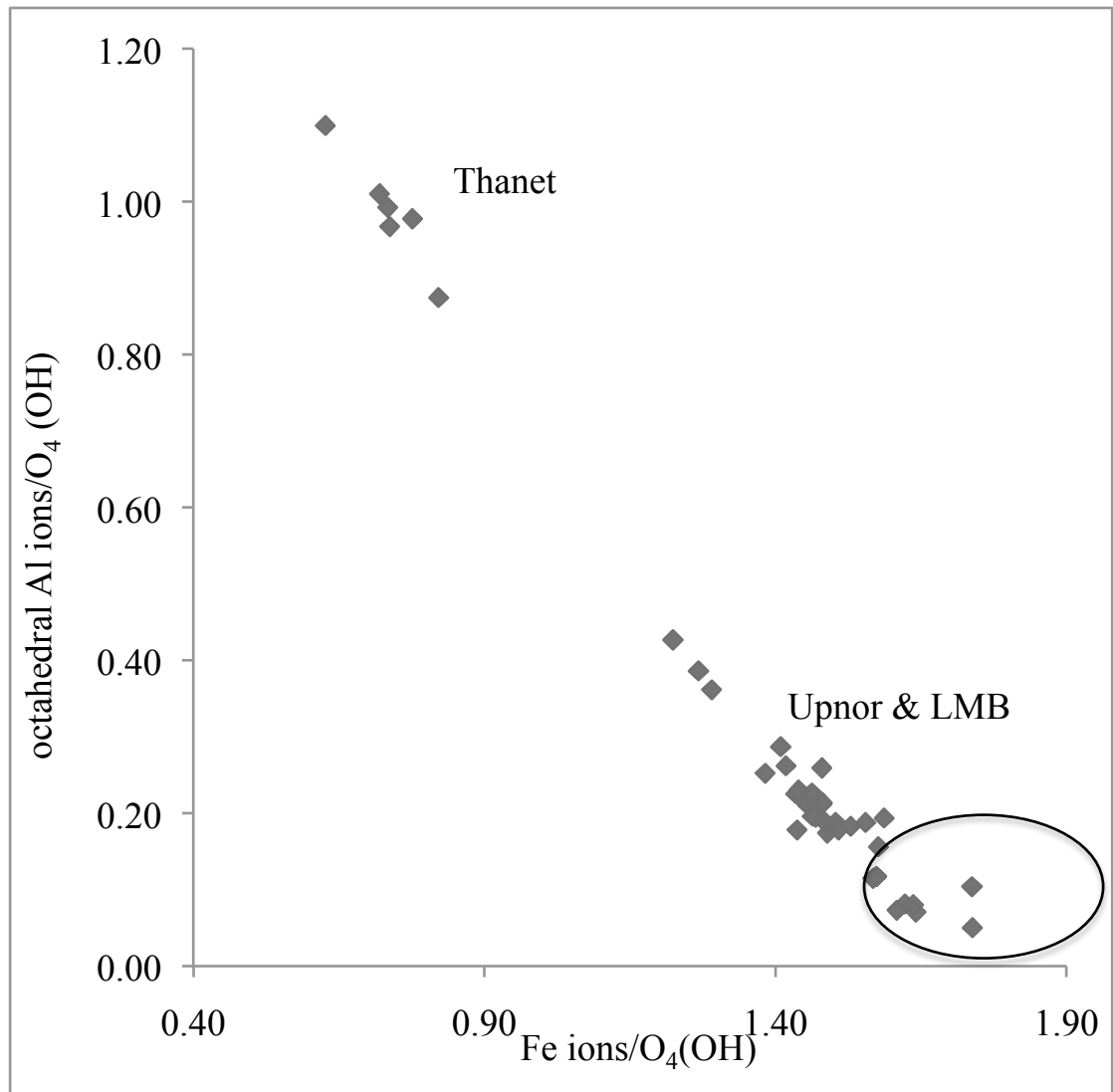


Fig 7

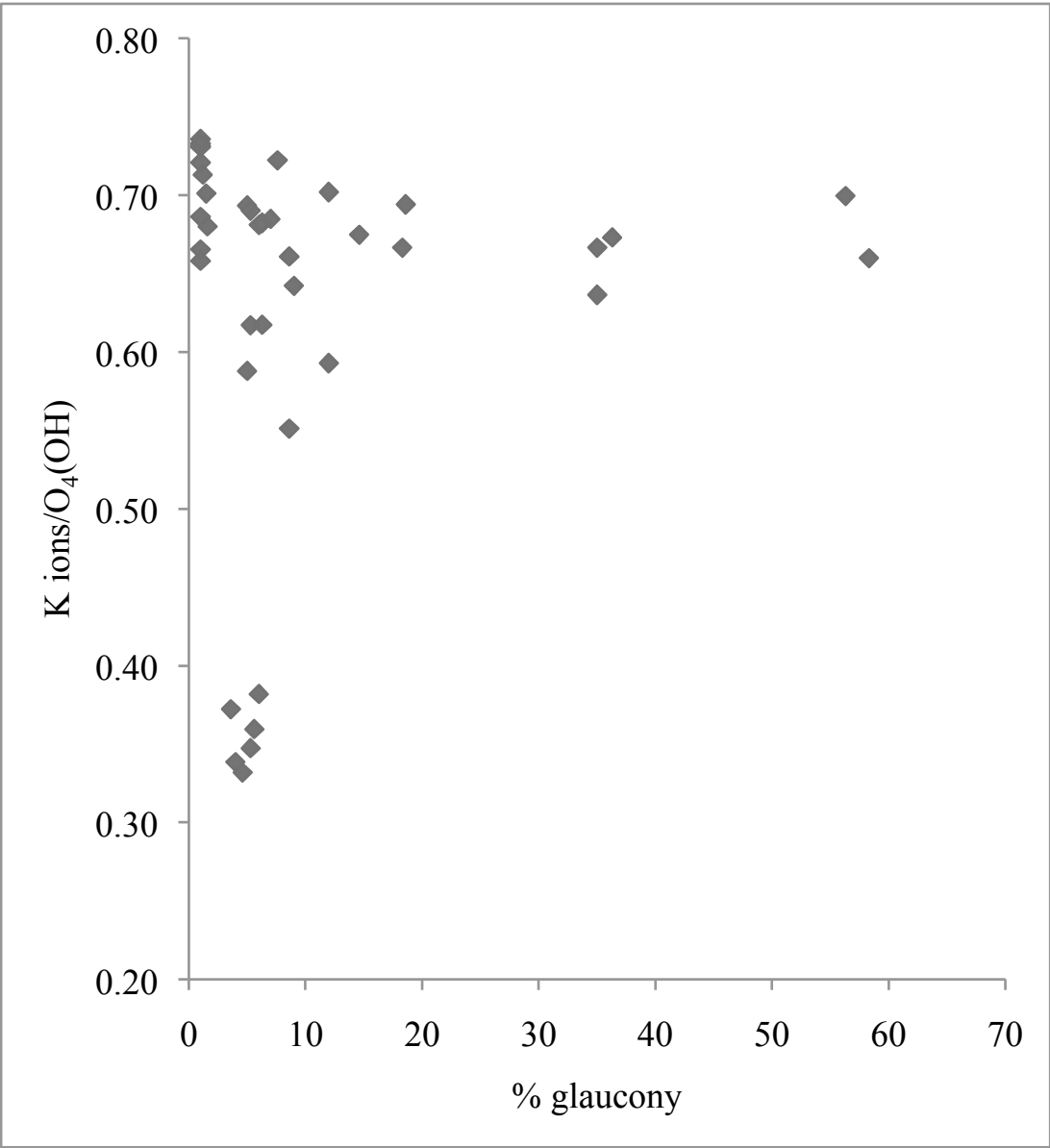


Fig 8

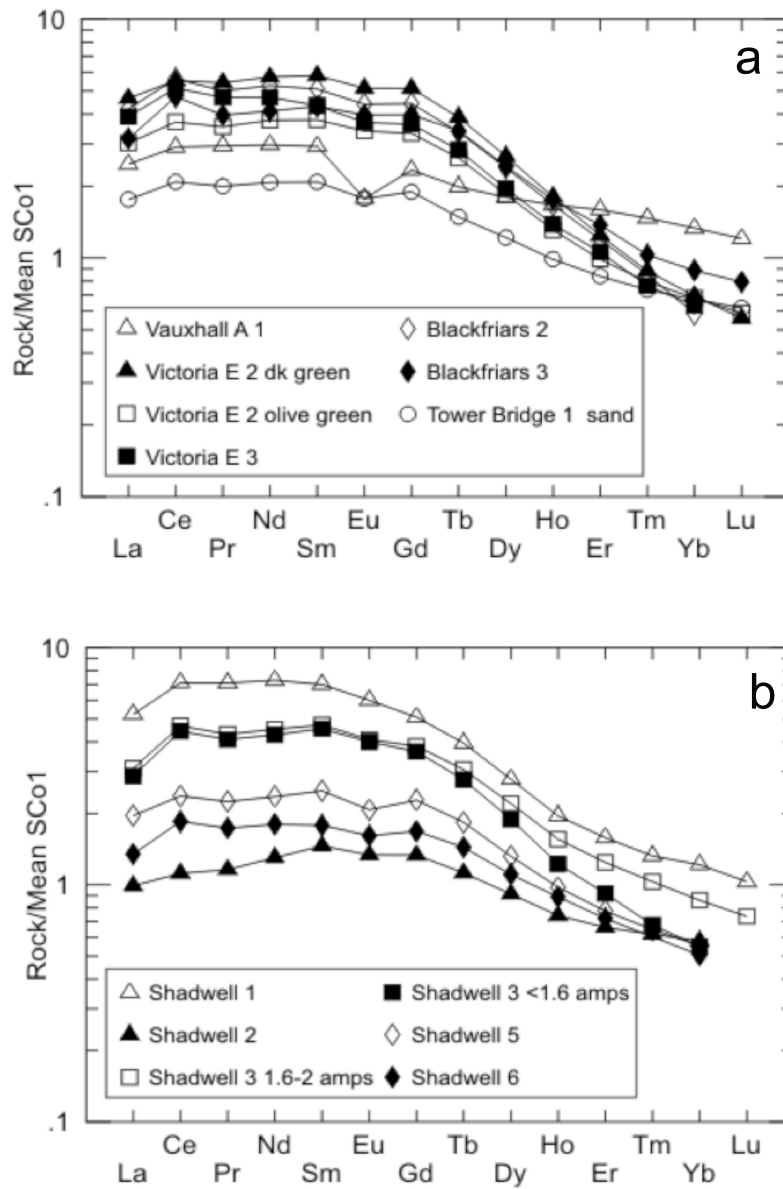


Fig 9a-b

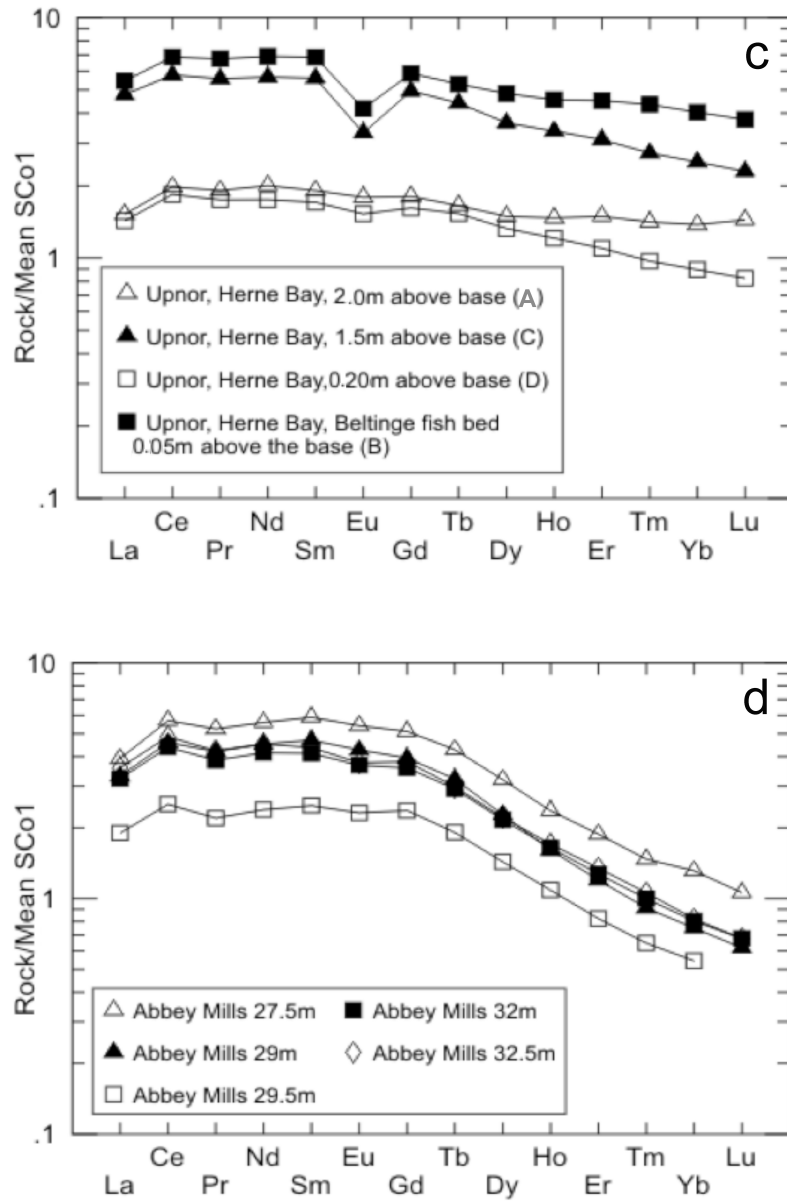


Fig 9c-d

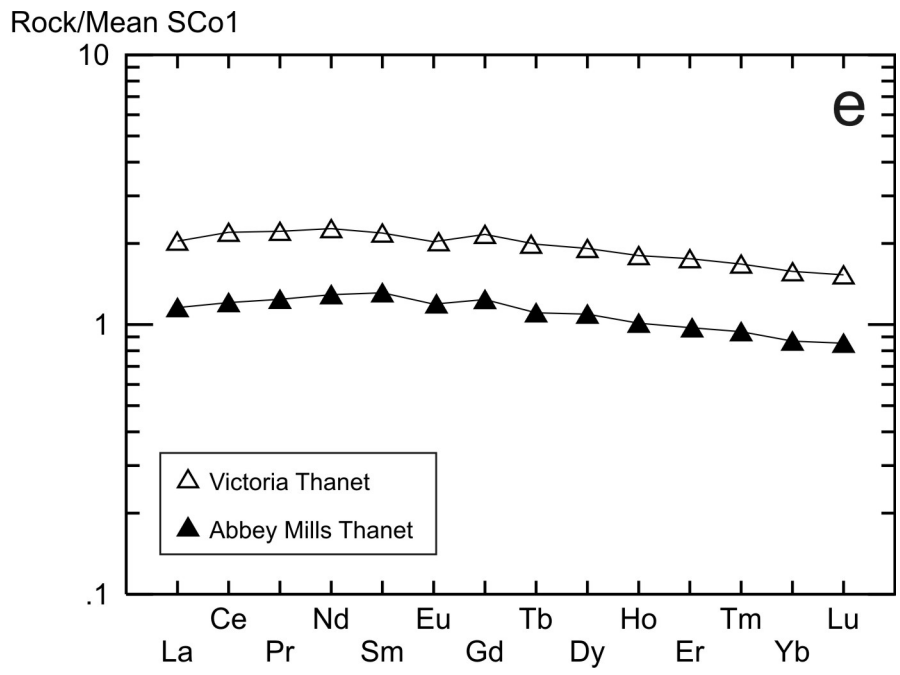


Fig 9e

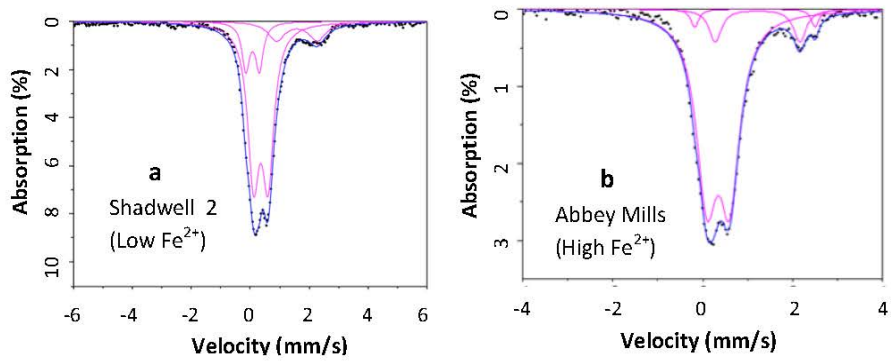


Fig. 10

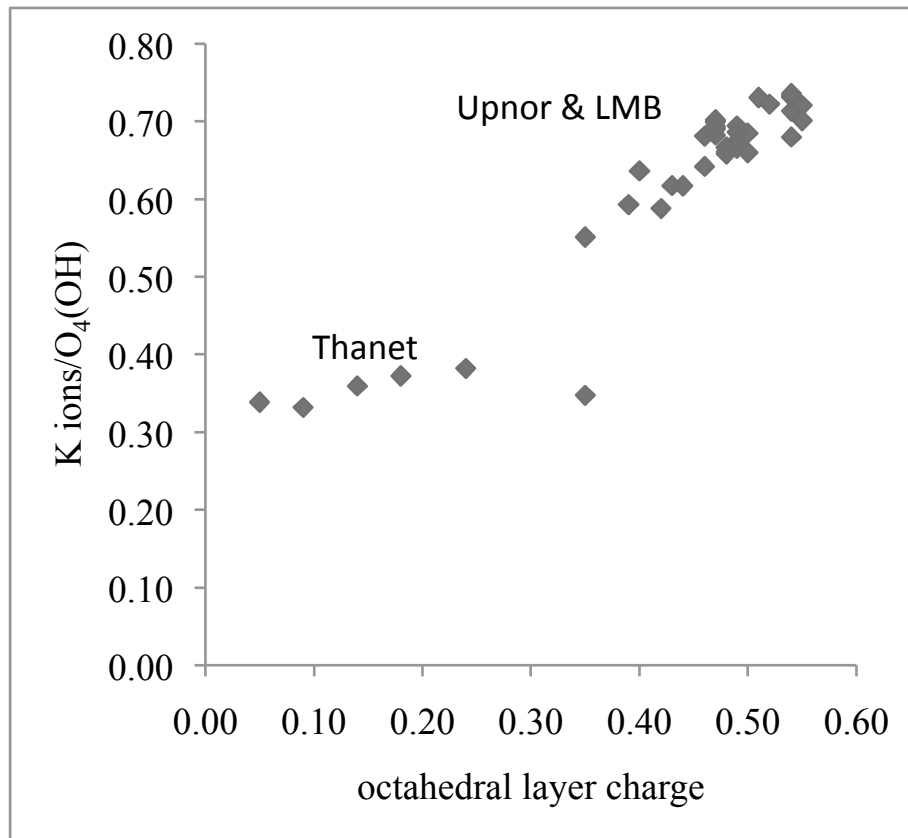


Fig.

11a

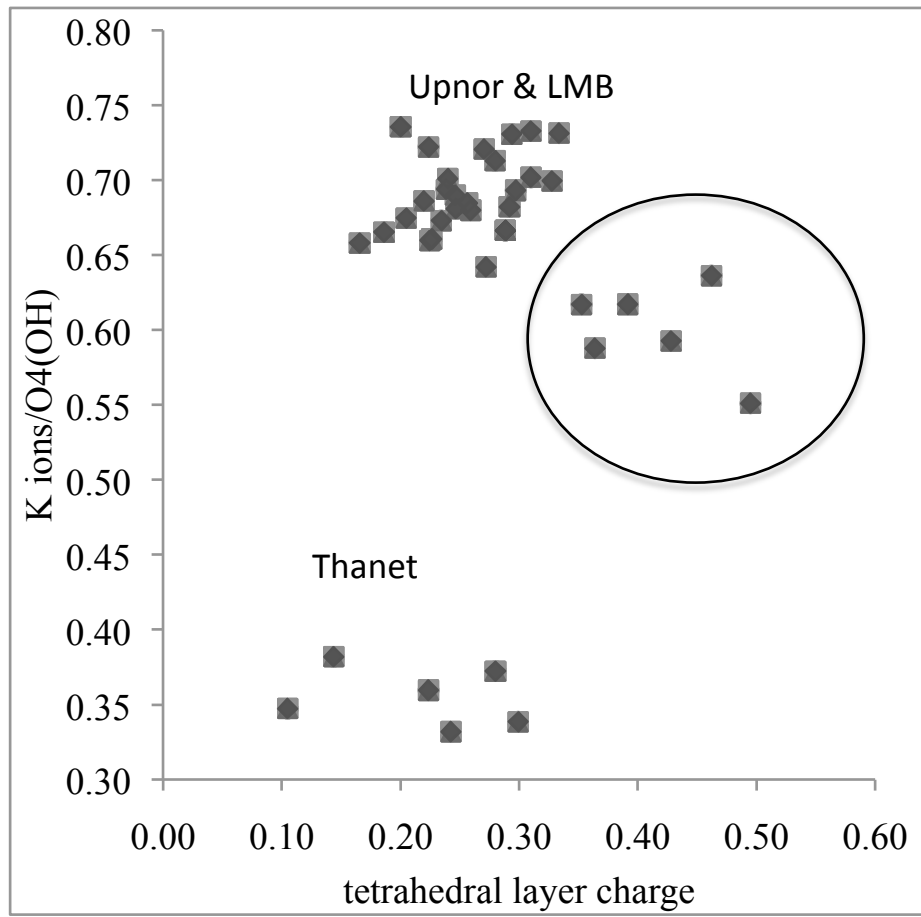


Fig. 11b

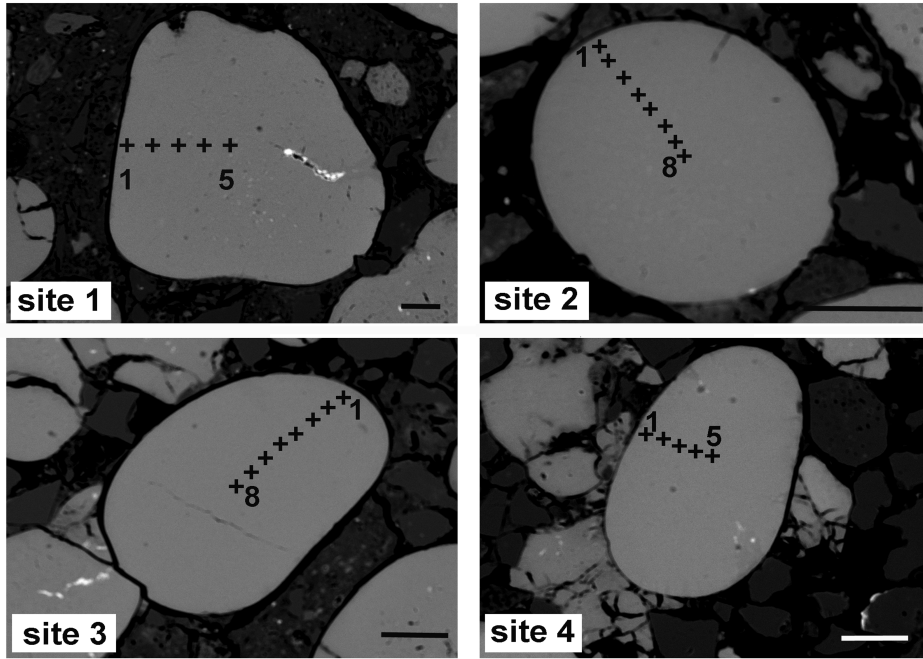


Fig. 12

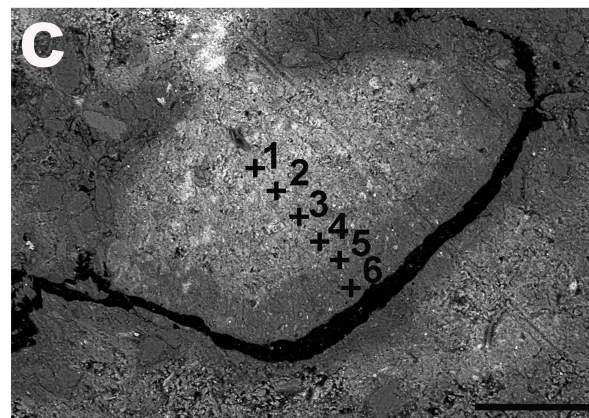
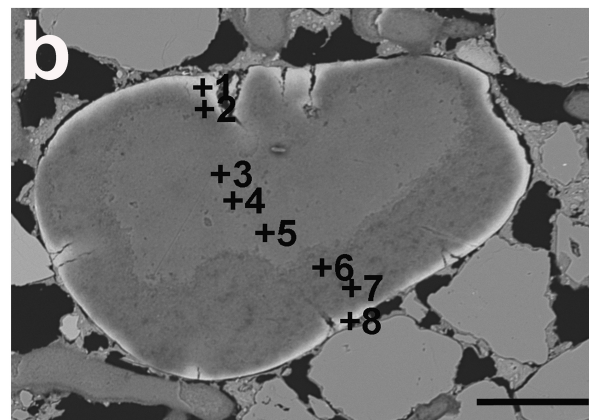
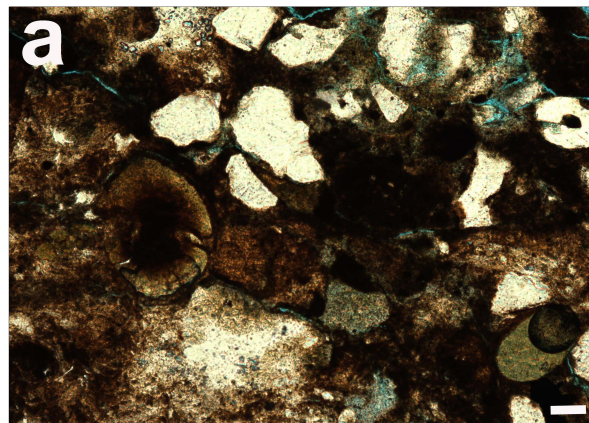


Fig. 13

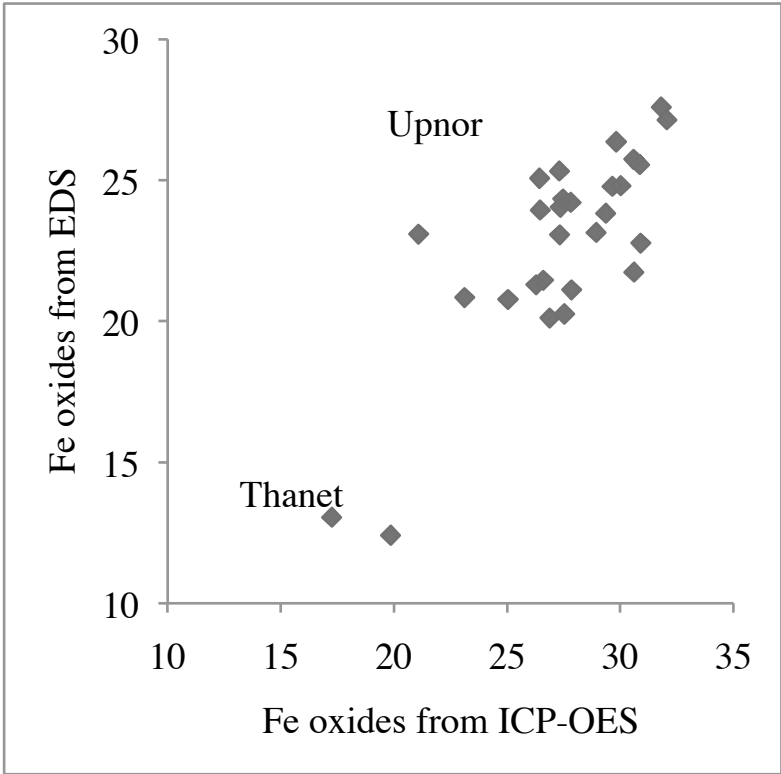
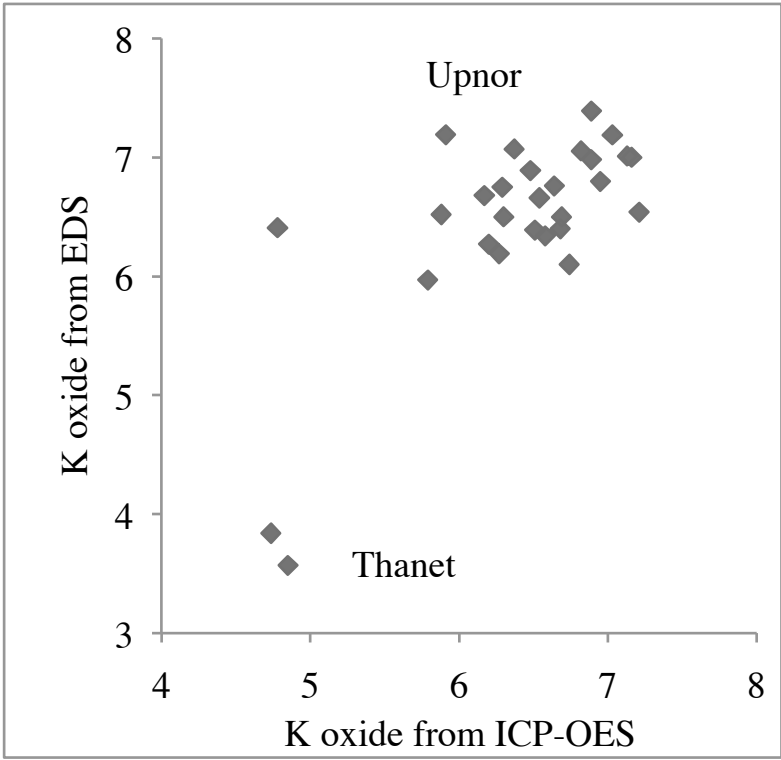


Figure 14

Sample	Species	Location	$\delta^{13}\text{C}$	9
			‰ VPDB	
oyster shell	<i>Ostrea bellovacina</i>	Abbey Mills, 30.5 m	<b>-1.7</b>	
shark tooth	<i>Striatolamia striata</i>	Beltinge Fish Bed, Herne Bay, Kent		
shark tooth	<i>Glueckmanotodus heinzelini</i> (Casier 1967)	Beltinge Fish Bed, Herne Bay, Kent		
shark tooth	<i>Palaeohypotodus rutoti</i>	Beltinge Fish Bed, Herne Bay, Kent		
shark tooth	<i>Otodus obliquus</i>	Beltinge Fish Bed, Herne Bay, Kent		
shark tooth	<i>Myliobatis</i> sp	Beltinge Fish Bed, Herne Bay, Kent		
calcite; <sup>2</sup> phosphate oxygen extracted from enameloid for all shark teeth				
values in bold font are averages of duplicate analyses				

Table 1

Site	Spectrum	Compound oxide weight %								Normalised oxide weight%				
		SiO <sub>2</sub>	Al <sub>2</sub> O <sub>3</sub>	Fe <sub>2</sub> O <sub>3</sub>	CaO	MgO	Na <sub>2</sub> O	K <sub>2</sub> O	Total	SiO <sub>2</sub>	Al <sub>2</sub> O <sub>3</sub>	Fe <sub>2</sub> O <sub>3</sub>	CaO	MgO
1	1	47.1	2.4	27.4	0.0	3.0	0.0	7.7	87.6	53.8	2.8	31.2	0.0	3.4
	2	49.3	1.9	28.1	0.0	3.4	0.0	7.7	90.4	54.6	2.1	31.1	0.0	3.7
	3	49.7	2.2	28.0	0.0	3.2	0.0	7.4	90.4	54.9	2.5	30.9	0.0	3.5
	4	50.2	2.3	27.7	0.0	3.1	0.0	7.6	90.8	55.2	2.5	30.5	0.0	3.4
	5	49.6	2.3	27.9	0.0	3.2	0.0	7.4	90.3	54.9	2.5	30.9	0.0	3.5
2	1	47.5	5.1	23.0	0.0	3.1	0.0	7.2	85.9	55.3	6.0	26.7	0.0	3.6
	2	49.5	4.5	23.4	0.0	3.2	0.0	7.6	88.2	56.1	5.1	26.6	0.0	3.6
	3	50.0	4.4	25.2	0.0	3.1	0.0	7.5	90.1	55.5	4.9	27.9	0.0	3.4
	4	49.7	4.1	25.3	0.0	3.1	0.0	7.5	89.6	55.5	4.5	28.3	0.0	3.4
	5	49.1	3.8	25.2	0.0	3.1	0.0	7.5	88.6	55.4	4.3	28.4	0.0	3.5
	6	50.4	3.6	25.9	0.0	3.1	0.0	7.6	90.6	55.6	4.0	28.6	0.0	3.4
	7	50.2	3.7	26.2	0.0	3.0	0.0	7.5	90.7	55.4	4.1	28.9	0.0	3.3
	8	50.1	3.3	25.9	0.0	3.3	0.0	7.7	90.2	55.5	3.7	28.7	0.0	3.6
3	1	50.1	2.4	26.2	0.0	3.1	0.0	8.0	89.7	55.8	2.7	29.2	0.0	3.4
	2	50.1	2.0	27.5	0.0	3.1	0.0	7.9	90.6	55.3	2.2	30.3	0.0	3.4
	3	50.0	2.0	27.2	0.0	3.2	0.0	7.8	90.2	55.4	2.2	30.1	0.0	3.5
	4	50.4	2.1	27.7	0.0	3.3	0.0	7.9	91.5	55.1	2.3	30.3	0.0	3.7
	5	50.6	2.0	27.3	0.0	3.2	0.0	7.9	91.0	55.6	2.2	30.0	0.0	3.5
	6	50.7	1.9	27.7	0.0	3.3	0.0	7.9	91.4	55.4	2.0	30.2	0.0	3.6
	7	50.7	1.8	27.5	0.0	3.3	0.0	8.0	91.3	55.5	2.0	30.1	0.0	3.7
	8	50.4	1.9	27.5	0.0	3.2	0.0	8.0	91.0	55.4	2.1	30.2	0.0	3.5
4	1	46.5	4.8	25.5	0.0	3.0	0.0	7.1	86.8	55.2	4.6	28.8	0.0	3.5
	2	48.9	4.1	25.4	0.0	3.1	0.0	7.6	89.1	55.4	4.4	28.3	0.0	3.6
	3	49.8	4.1	26.1	0.0	3.3	0.0	7.3	90.5	55.0	4.5	28.8	0.0	3.7
	4	49.5	3.9	25.3	0.0	3.2	0.0	7.4	89.3	54.9	4.6	28.5	0.0	3.5
	5	50.0	4.1	26.0	0.0	3.2	0.0	7.2	90.6	53.6	5.5	29.4	0.0	3.4

Table 2

		Compound oxide weight %								
Site 1	Spectrum	SiO <sub>2</sub>	Al <sub>2</sub> O <sub>3</sub>	Fe <sub>2</sub> O <sub>3</sub>	P <sub>2</sub> O <sub>5</sub>	CaO	MgO	Na <sub>2</sub> O	K <sub>2</sub> O	Total
	1	48.2	5.5	22.8	0.0	1.3	3.3	0.0	7.2	88.3
	2	24.0	40.2	11.4	0.0	0.6	1.0	0.9	3.6	81.6
	3	15.7	55.3	6.7	0.0	0.8	0.0	0.9	2.0	81.3
	4	11.8	61.9	5.1	0.0	0.6	0.0	0.8	1.7	81.7
	5	10.4	61.7	4.7	0.0	0.5	0.0	0.7	1.5	79.5
	6	16.9	53.5	7.6	0.0	0.6	0.5	0.9	2.4	82.3
	7	19.2	45.5	9.1	0.5	0.5	0.7	0.7	3.0	79.1
	8	50.4	6.4	22.5	0.0	0.0	3.3	0.0	7.4	90.0
Site 2	Spectrum	SiO <sub>2</sub>	Al <sub>2</sub> O <sub>3</sub>	Fe <sub>2</sub> O <sub>3</sub>	P <sub>2</sub> O <sub>5</sub>	CaO	MgO	Na <sub>2</sub> O	K <sub>2</sub> O	Total
	1	29.3	14.4	14.2	0.0	0.4	1.4	0.0	2.2	61.9
	2	33.3	15.4	16.9	0.0	0.5	1.4	0.0	2.6	70.0
	3	39.6	15.4	19.9	0.0	1.4	1.5	0.0	2.6	80.3
	4	36.0	17.3	23.8	0.0	0.8	1.8	0.0	3.0	82.6
	5	37.8	15.8	15.7	0.0	0.5	1.3	0.0	2.3	73.4
	6	36.6	15.7	15.4	0.0	1.1	1.5	0.0	2.8	73.0
		Normalised oxide weight%								
Site 1	Spectrum	SiO <sub>2</sub>	Al <sub>2</sub> O <sub>3</sub>	Fe <sub>2</sub> O <sub>3</sub>	P <sub>2</sub> O <sub>5</sub>	CaO	MgO	Na <sub>2</sub> O	K <sub>2</sub> O	
	1	54.6	6.2	25.9	0.0	1.5	3.7	0.0	8.1	
	2	29.5	49.3	13.9	0.0	0.7	1.2	1.1	4.4	
	3	19.2	68.0	8.2	0.0	0.9	0.0	1.1	2.5	
	4	14.4	75.7	6.3	0.0	0.7	0.0	0.9	2.0	
	5	13.1	77.6	6.0	0.0	0.6	0.0	0.8	1.9	
	6	20.5	65.0	9.2	0.0	0.8	0.6	1.0	2.9	
	7	24.3	57.6	11.5	0.5	0.6	0.9	0.8	3.8	
	8	56.0	7.1	25.0	0.0	0.0	3.6	0.0	8.3	
Site 2	Spectrum	SiO <sub>2</sub>	Al <sub>2</sub> O <sub>3</sub>	Fe <sub>2</sub> O <sub>3</sub>	P <sub>2</sub> O <sub>5</sub>	CaO	MgO	Na <sub>2</sub> O	K <sub>2</sub> O	
	1	47.3	23.2	23.0	0.0	0.7	2.2	0.0	3.5	
	2	47.5	22.0	24.1	0.0	0.6	2.0	0.0	3.7	
	3	49.3	19.1	24.8	0.0	1.8	1.8	0.0	3.2	
	4	43.5	20.9	28.7	0.0	1.0	2.2	0.0	3.7	
	5	51.5	21.5	21.3	0.0	0.7	1.8	0.0	3.2	
	6	50.1	21.5	21.0	0.0	1.5	2.0	0.0	3.8	

Table 3